

Kinematics and time-resolved evolution of the main thrust-sense shear zone in the Eo-Alpine orogenic wedge (the Vinschgau Shear Zone, Eastern Alps)

5 Chiara Montemagni¹, Stefano Zanchetta¹, Martina Rocca¹, Igor M. Villa¹, Corrado Morelli², Volkmar Mair², Andrea Zanchi¹

1 Dipartimento di Scienze dell’Ambiente e della Terra, Università degli Studi di Milano – Bicocca, Milano, 20126, Italia

2 Ufficio Geologia e Prove Materiali, Provincia Autonoma di Bolzano Alto Adige, Cardano, 39053, Italia

10 *Correspondence to:* chiara.montemagni@unimib.it

Abstract

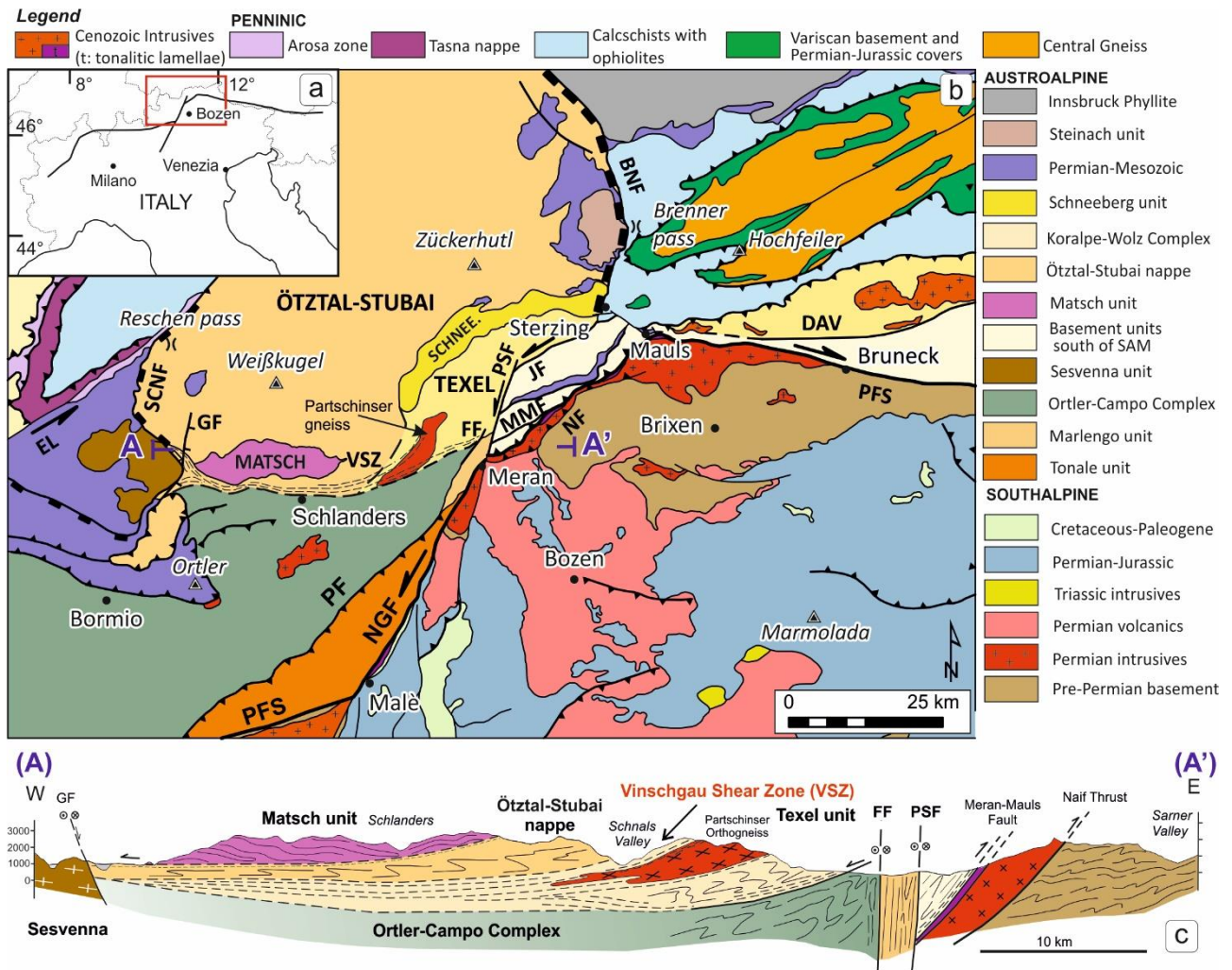
The Vinschgau Shear Zone (VSZ) is one of the largest and most significant shear zones developed in plastic conditions within the Austroalpine domain, juxtaposing the Ötztal and the Texel units to the Campo, Scharl and Sesvenna units during the building of the Eo-Alpine Orogen. The VSZ dominates the structural setting of a large portion of the central Austroalpine Late Cretaceous thrust stack. In order to fully assess the evolution of the VSZ, a multi-faceted approach based on detailed multiscale structural and petrochronological analyses has been carried out across representative transects of the shear zone in the Vinschgau Valley. The research has been performed with a view to characterizing kinematics, *PT* conditions and age of motion of the VSZ.

20 Our fieldwork-based analyses suggest that the dip of mylonitic foliation increases from W to E with an E-W trending stretching lineation which dips alternatively to the W and to the E, due to later folding related to the Cenozoic crustal shortening. The dominant top to the W-directed shear sense of the mylonites recognized in the field and confirmed by microstructural analyses led to exhumation of the upper Austroalpine nappes in the hanging wall of the shear zone: the Texel unit with Late Cretaceous eclogites, the Schneeberg and Ötztal units both affected by Eo-Alpine amphibolite-facies metamorphism. Chemical and microstructural analyses suggest deformation temperatures of ca. 350-400 °C during shearing. Timing of deformation along the VSZ has been constrained for the first time through ⁴⁰Ar/³⁹Ar dating of syn-shearing micas, which reveal a Late Cretaceous age of the VSZ mylonites with ages ranging between 80 and 97 Ma. A systematic younging age of deformation occurs towards the central part of the shear zone in the studied transects. Vorticity analysis shows a clear decrease in the simple shear component correlated to the younging direction of mica ages towards the core of the shear zone. This evolution is consistent with the growth of a shear zone where shear strain localizes into its central part during deformation. The defined evolution of the VSZ sheds new light on how large-scale thrust-sense shear zones act and how much exhumation they can accommodate in the frame of an evolving orogenic wedge.

1. Introduction

35 The Vinschgau Shear Zone (VSZ), extending along the homonymous valley (NE Italy; Fig. 1a-b), is one of the most important tectonic structures developed within the Austroalpine domain of the Alps (Fig. 1 and Fig. 2). Starting from the first systematic studies of the Alpine belt, this large shear zone, firstly defined as the “Schlinig Thrust”, was interpreted as a top-to-W thrust plane (Spitz and Dyhrenfurth, 1914). Although several authors later rejected this interpretation (Heim, 1922; Staub, 1937), modern studies (Schmid and Haas, 1989; Froitzheim et al., 1994, 1997) carried out since the end of the last century demonstrated the validity of the first assumptions. Recent structural analyses (Brunel, 1980; Ratschbacher, 1986, Ratschbacher et al., 1989; Schmid and Haas, 1989; Pomella et al., 2016) recognized indeed that the entire central Austroalpine nappe stack was affected by W-directed tectonic transport during the first stages of the Late Cretaceous Alpine deformations. Along the VSZ, the Austroalpine tectonometamorphic units with a dominant metamorphism of Alpine age overthrust Austroalpine units (Sesvenna and Campo-Ortler) that were only slightly affected by Alpine

45 metamorphism (up to greenschist facies) and deformation during the Eo-alpine stage (Thöni, 1981), still largely preserving features acquired during the Variscan orogeny.



50 **Figure 1: Geological setting of the eastern-central Alps. (a)** Northern Italy, location of the study area is marked with a red box; **(b)** Tectonic scheme of the eastern-central Alps (modified after Schmid et al., 2004; Pomella et al., 2016). **(c)** The cross section, trace A-A' in figure (a), has been drawn in a larger scale with respect of the tectonic scheme. BNF: Brenner Normal Fault; DAV: Defereggan-Antholz-Vals Fault; EL: Engadine Line; FF: Forst Fault; GF: Glurns Fault; JF: Jaufen Fault; NGF: North Giudicarie Fault; PF: Pejo Fault; PFS: Periadriatic Fault; PSF: Passeier Fault; SCNF: Schling Normal Fault; VSZ: Vinschgau Shear Zone.

55 The VSZ is almost continuously exposed for more than 50 km, mainly on the northern flank of the Vinschgau Valley (Fig. 1), reaching a maximum thickness of about 550 m close to Eyrs (Fig. 1 and Fig. 2). These features make the VSZ one of the largest ductile thrust-sense shear zone now exposed in the Alps, together with the Periadriatic Fault (Schmid et al., 1987; 1989) and the Orobic Thrust in the Southern Alps (Zanchetta et al., 2011; D'Adda and Zanchetta, 2015). The Noric Thrust in the Eastern Alps (Ratschbacher, 1986) is another important ductile thrust, the first one studied by modern kinematic and structural methods. Due to its complete exposure and accessibility, the prominent VSZ represents an ideal natural laboratory for the study of cumulative shear strain distribution during the development of a large mature intra-basement shear zone and to evaluate the evolution in terms of shear strain localization, coaxiality, kinematic, and lifetime of activity (e.g. Xypolias, 2010; Xypolias and Koukouvelas, 2001; Law et al., 2013; Fossen and Cavalcante, 2017; Oriolo et al., 2016, 2018).

60

65

Large scale thrust- or normal-sense shear zone developed within collisional setting display huge along-strike exposures as the ca. 2500 km of the Main Central Thrust and South Tibetan Detachment in the Himalayan orogen (e.g. Caby et al., 1983; Searle et al., 2008), the ca. 30 km of the Simplon Shear Zone (Mancktelow, 1985) and Brenner Fault (Rosenberg et al., 2018) in the Alps or the Great Slave Lake shear zone (Hamner et al., 1992) in northern Canada. Due to its peculiar exposure along strike, the VSZ shows different features from shallow depths conditions at its western portion and deeper conditions at the eastern end (Schmid and Haas, 1989), providing a complete crustal section of a large scale shear zone. This kind of exposure provides insights not only on the different deformation mechanisms and behaviours of the shear zone at different crustal levels, but also on its evolution through time.

In this work, we applied a quantitative approach to reconstruct the evolution through space (depth) and time of the VSZ. $^{40}\text{Ar}/^{39}\text{Ar}$ dating of syn-mylonitic micas sampled along several transects of the VSZ have been combined with microstructural and mineralogical analyses, aimed to define the *PT* condition of shearing. The analysis of the cumulative shear strain distribution and the kinematic vorticity of flow (e.g. Montemagni and Zanchetta, 2022; Petroccia et al., 2022) finally provide a full kinematic and time-resolved evolution of the VSZ, that could be taken as an example of how a large-scale thrust-sense shear zone develops within a collisional orogen.

80

2. Geological setting

The study area (Fig. 1 and Fig. 2) is located along the Vinschgau Valley (NE Italy) entirely extending within the central Austroalpine domain, comprised between the Northern Calcareous Alps to the north and the Periadriatic Fault to the south (Fig. 1). Here, the Austroalpine domain consists of tectono-metamorphic units that have been identified based on paragenesis, deformation history, metamorphism and relative ages. These units are the Pejo and Laas units (belonging to the Campo-Ortler nappe system), and the Ötztal-Stubai Complex, the Matsch unit, and, finally, the Texel and the Schneeberg units, belonging to the Koralpe-Wölz high-pressure nappe system (Schmid et al., 2004; Handy et al., 2010; Pomella et al., 2016; Klug and Froitzheim, 2022). The E-W striking VSZ separates the Pejo and Laas units to the south, the footwall of the VSZ characterized by greenschist facies Alpine metamorphism, from the Ötztal, Matsch, Texel and Schneeberg units forming the hanging wall, characterized by amphibolite to eclogite facies Alpine metamorphism (Fig. 2). Therefore, the VSZ together with the Passeier Fault, the Jaufen Fault and the Deferegggen-Antholz-Vals Fault (PSF, JF and DAV in Fig. 1) has been considered to form the Southern limit of Alpine Metamorphism (SAM, Hoinkes et al., 1999), a large faults system defining the southern border of the high-grade Alpine metamorphism in the Austroalpine domain of the Eastern Alps.

90

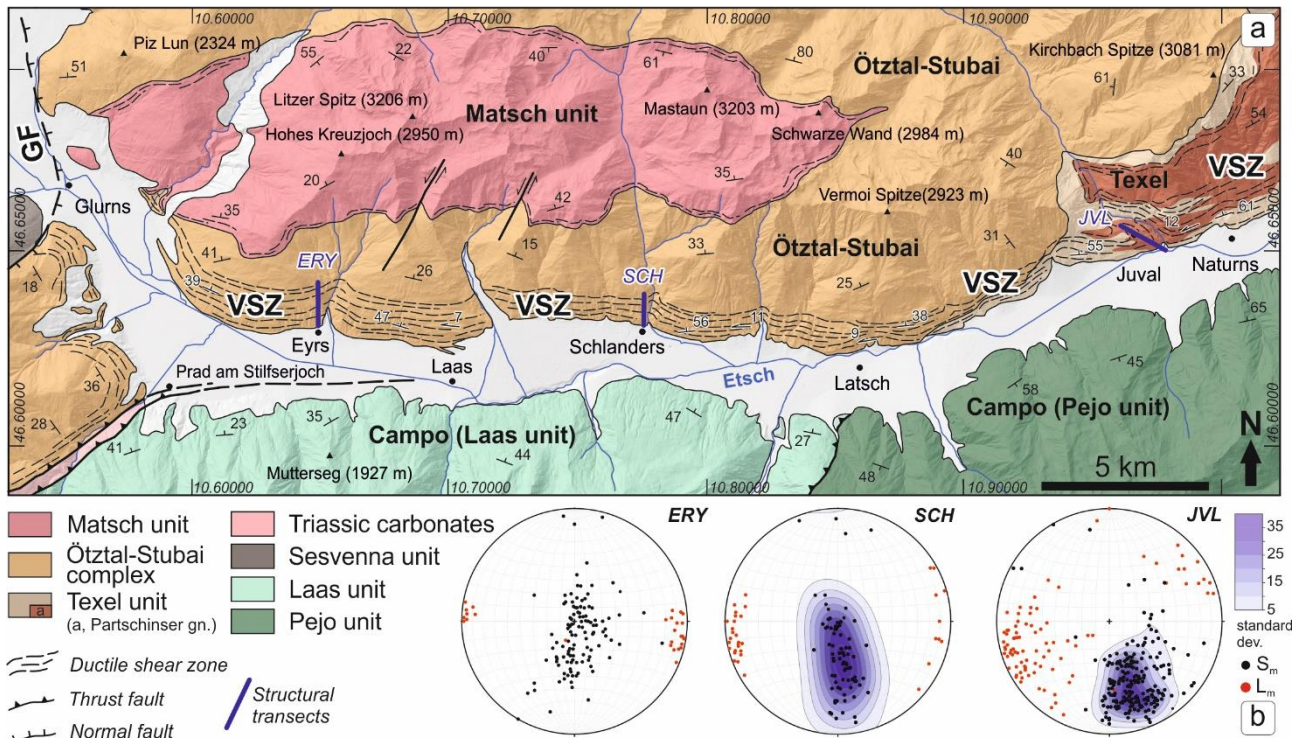


Figure 2: (a) Tectonic scheme of the Vinschgau Valley, the location of studied transects (ERY, SCH and JVL) has been reported. (b) Structural data of Eyrns, Schlanders and Juval transects, equal area, lower hemisphere stereographic projections of mylonitic foliation (S_m) and lineation (L_m); Kamb contours are represented as standard deviation. GF: Glurns Fault; VSZ: Vinschgau Shear Zone.

The VSZ has been described as a ductile-to-brittle fault formed by a thick zone of mylonites and phyllonites exposed mainly along the left hydrographic side of the Vinschgau Valley (Fig. 2; Schmid and Haas, 1989; Conti, 1994; Froitzheim et al., 1997; Thöni, 1999; Sölvä et al., 2005; Pomella et al., 2016; Koltai et al., 2018; Klug and Froitzheim, 2022). Schmid and Haas (1989) defined the main structure as a thick intrabasement shear zone dominated by intracrystalline plastic processes, showing different thermal conditions ranging from 300 °C to the west up to 500 °C to the east. The VSZ forms a wide system of shear zones, branching out eastward across the folded boundaries between the Ordovician Partschinser Granodiorite (also named Tschigot orthogneiss, Zantedeschi, 1991) and the host paragneiss of the Texel unit. The VSZ shows a gently N-dipping foliation (20°-30°) and a constantly E-W trending lineation, with kinematic indicators at the mesoscopic and microstructural scale that point to a top-to-N/NW sense of shear (Schmid and Haas, 1989).

Four tectonic units mainly consisting of polyphase metamorphic crystalline basement rocks, which have been deeply involved in the Alpine deformation and metamorphism, form the hanging wall of the shear zone. They consist of the western termination of the Texel and Schneeberg units, and of the Ötztal unit, one of the largest nappes of the Late Cretaceous Austroalpine thrust stack, which is overthrust by the Matsch unit, forming a folded klippe atop of the VSZ mylonites.

The age pattern of the Alpine metamorphic peak of the tectonometamorphic units in the hanging wall of the VSZ displays almost coeval ages in the Texel and the Schneeberg units. Partially amphibolitized eclogite boudins, preserved within the micaschists and paragneisses of the Texel unit, point to metamorphic peak conditions during the Alpine orogenesis of 540-630 °C and 1.2-1.4 GPa (Habler et al., 2006), with even higher temperature and pressure suggested for other eclogite occurrences (Poli, 1991; Zanchetta et al., 2012; Zanchetta et al., 2013). Peak metamorphic conditions close to the amphibolite/eclogite facies boundary have been suggested for the Schneeberg unit, with peak temperature of 550-600 °C, at pressure of 0.8-1.0 GPa (Konzett and Hoinkes, 1996; Krenn et al., 2011). Geochronological data point to a Late Cretaceous age for both the Texel eclogites (U-Pb zircon ages of 84 ± 5 Ma; Habler et al., 2006; Zanchetta et al., 2013) and the upper amphibolite facies metamorphism of the Scheneberg unit, for which ages ranging between 85-86 Ma

125 ($^{40}\text{Ar}/^{39}\text{Ar}$ age on paragonitic white mica in amphibolites, Konzett and Hoinkes, 1996) and 90.9 ± 4.1 Ma (Sm-Nd on garnet cores in metapelites, Sölva et al., 2005) have been obtained.

The age and the peak metamorphic conditions experienced by the Ötztal unit during the Alpine metamorphism are far less constrained. Mid to Late Cretaceous K-Ar mica ages (100-110 Ma) have been obtained by Thöni (1980) from the basement in the hanging wall of the VSZ and a whole rock Rb-Sr age of 83 ± 1 Ma resulted from a metapegmatite of the Matsch unit (Fig. 2) at the western end of the VSZ (Thöni, 1986). An Alpine age of upper greenschist facies metamorphism in the Matsch unit has been also argued by Habler et al. (2009), on the base of Early to Middle Permian intrusions age of pegmatites, later deformed and metamorphosed, and the growth of chloritoid after pre-Alpine staurolite. The Alpine metamorphism in the Ötztal unit reached 530-550 °C in the southeastern part (Purtscheller and Rammlmair, 1982; Hoinkes et al. 1999), with temperatures that progressively decrease toward NW. Pressure estimates are substantially lacking. On the base of newly formed mineralogical assemblages in pre-Alpine andesitic and andesitic/basaltic dikes intruding the Ötztal basement, Purtscheller and Rammlmair (1982) supposed a maximum pressure of about 0.5-0.6 GPa, confirmed by recent data (Zanchetta et al., 2013). Additional *PT* estimates have been proposed by Gregnanin and Valle (1995) for the Ötztal metasedimentary cover (550 °C and 1.0 GPa), and by Tropper and Reichis (2009) for the SW part of the Ötztal basement (560 °C and 0.88 GPa) close to the Schneeberg unit.

140 The westernmost portion of the VSZ is crosscut by the Glurns Fault (GF in Fig. 2), along which the Ötztal basement is in contact with the Sesvenna unit, mainly consisting of orthogneiss with a Variscan medium-grade metamorphic imprint and its Permian-Mesozoic sedimentary cover (Froitzheim et al., 1994; 1997).

3. Structural analysis

3.1. General description and methods

145 The entire VSZ has been individuated and followed in the field from Naturns (E) to Glurns (W) (Fig. 2). The maximum thickness is reached close to its western ends, at Eyrs, where it is estimated to be of about 600 m. To the east of Naturns (Fig. 2) the VSZ widens and branches out in several shear zones that wrap around the rigid body of the Partschinser orthogneiss of the Texel unit, as already noticed by Schmid and Haas (1989), which has given a Rb-Sr radiometric age of about 450 Ma (Zantedeschi, 1991). Here, in the Meran area, the VSZ is crosscut by most recent shear zones and faults (Bargossi et al., 2010).

150 Detailed field structural analyses and sampling of the VSZ were performed along three selected transects (Fig. 2) in the localities, from E to W: Juval, Schlanders and Eyrs. The three studied geological sections were chosen through field surveys and structural analyses. They are considered to be representative of the entire VSZ at different depths of exposure (shallowest conditions at Eyrs and deepest at Juval) and offer also the possibility to study and sampling the shear zone in continuity, due to the good bedrock exposure. Each transect (Fig. 2) has been mapped at a 1:2,000 scale, identifying the distribution of protomylonites, mylonites and ultramylonites following the classification by Simpson and De Paor (1993). Sampling sites were accurately selected on the base of their representativity along the transects and the possibility they offered to perform microstructural and geochronological analyses.

3.1.1. The Juval transect

160 The easternmost transect is completely within the Texel unit. The cross section extends SE-NW, from the bottom of the Vinschgau valley to the Juval Castle. Here the road is entirely excavated in the bedrock, offering a continuous exposure of the entire shear zone. The bedrock mainly consists of granitoid orthogneiss (Partschinser orthogneiss) showing different mylonitization degrees. This transect almost corresponds to the westernmost termination of the Texel unit (Fig. 2). Besides the Partschinser orthogneiss, the Texel unit here consists of garnet, staurolite and kyanite bearing paragneiss that are also affected by mylonitization. They chiefly occur in the upper and central part of the transect, alternating with the orthogneiss. Some amphibolite boudins (Fig. 3d) are also exposed within the paragneiss along the road that takes to the Juval Castle. Paragneisses display a decrease in grain size with respect to the ones outside the VSZ, especially in the central part of the transect, where they can be classified as protomylonites. Analysis of the shear strain distribution highlights a symmetric increase, from rims to core, with ultramylonites and mylonites (Fig. 3) concentrated in the central

170

part of the shear zone, whereas protomylonitic textures mainly occur both close to the structurally higher and lower margins. The mylonitic foliation is defined by the SPO (Shape Preferred Orientation, Passchier and Trouw, 2005) of biotite. The mylonitic lineation visible in outcrops mainly consists of elongated quartz aggregates and aligned biotite crystals (see section 3.2 for details). Foliation dips towards NNW, with mylonitic lineations that are nearly horizontal trending ENE-WSW (Fig. 2b). Moving toward the core of the shear zone, the clast-matrix ratio decreases, as does the size of K-feldspar porphyroclasts (Fig. 3). Ultramylonites appear as dark-grey bands within mylonites, a few centimetres up to 3-4 metres in thickness (Fig. 3c). Quartz ribbons, a few millimetres in thickness and up to several decimetres in extension, frequently occur (Fig. 3e). Porphyroclasts are scarce within the ultramylonites, with a mean size not exceeding a few millimetres, whereas they commonly display a mean size of 20-30 mm outside the shear zone. Kinematic indicators represented by σ and δ clasts (Fig. 3b), antithetic bookshelves in K-feldspar porphyroclasts and SCC' fabric, invariably point to a top-to-W/WNW sense of shear.

3.1.2. The Schlanders transect

The Schlanders transect is located about 20 km to the W of the Juval section (Fig. 2). This section of the VSZ is entirely within the Ötztal polymetamorphic basement, here chiefly consisting of granitoid orthogneiss and minor two-mica paragneiss.

The upper portion of the structural transect extends outside the VSZ, where orthogneiss still preserve their metamorphic regional foliation of Variscan age (Schmid and Haas, 1989; Hoinkes et al., 1999; Thöni, 1999) gently dipping to the E. The cumulative shear strain distribution visible along this transect is symmetric, as was the case in the Juval section. Shear strain increases from the margins toward the core of the shear zone, with a decreasing grain size of both matrix and K-feldspar porphyroclasts. On the base of the matrix/clast ratio (Simpson and De Paor, 1993), the orthogneiss is protomylonitic. Only towards the core of the shear zone mylonitic bands occur, ranging in thickness from 10 to 50 centimetres. Ultramylonites, which are frequent along the Juval transect, here occur only as 2-10 centimetres thick bands, with a dark-grey colour and an intense grain-size reduction (Fig. 3f). The mylonitic foliation dips to NNW with a variable dip angle (Fig. 2b). Dip variations result from the occurrence of late stage S-facing folds with E-W trending fold axes that refold the mylonitic foliation. The lineation associated to top-to-W shearing is nearly sub-horizontal or gently dipping to W (Fig. 2b), identified in the field by elongate quartz aggregates and white micas.

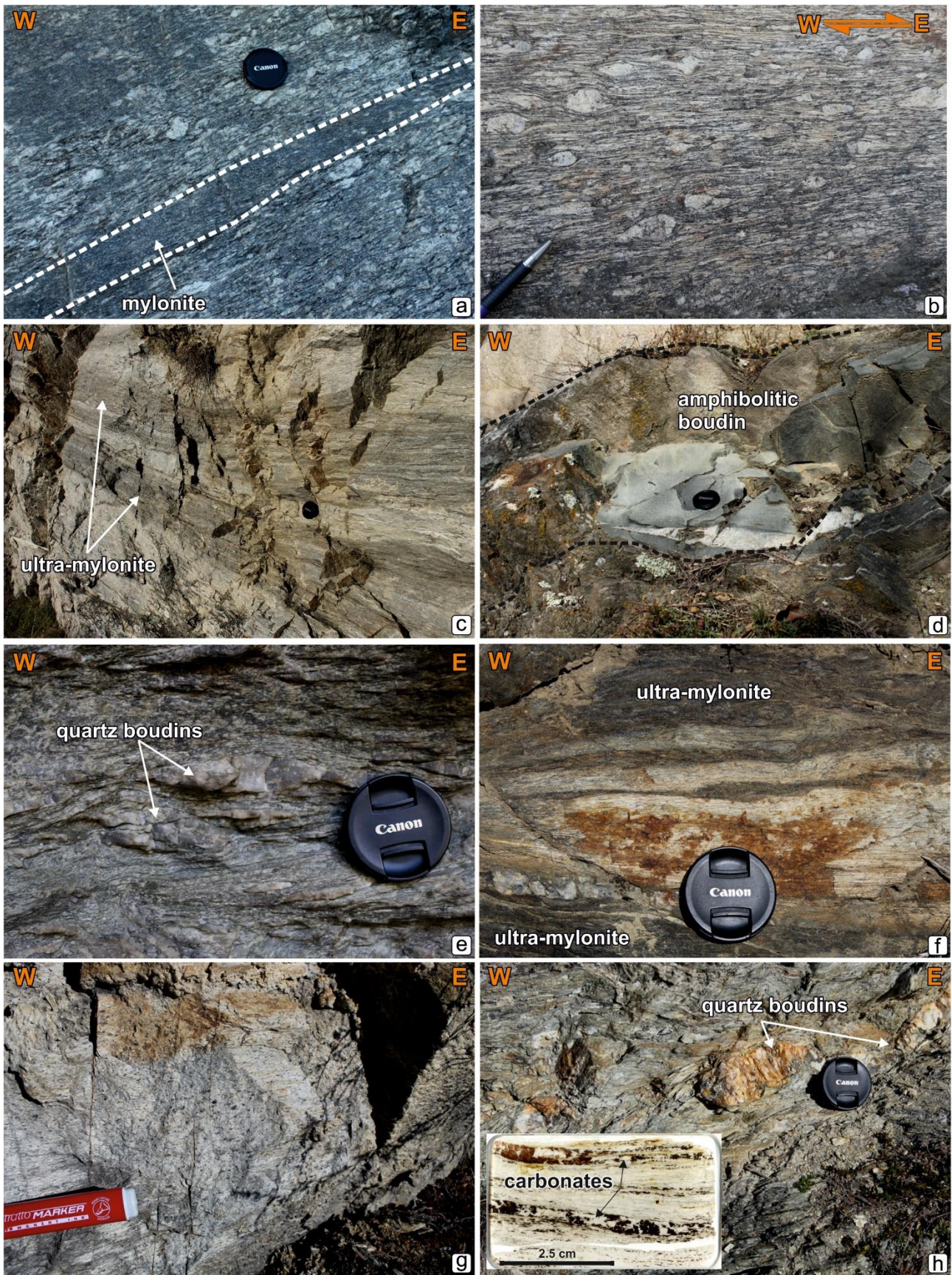


Figure 3: Field photographs of Juval, Schlanders and Eysr outcrops. (a) Proto-mylonitic Partschinser Orthogneiss with a mylonite band, recognizable from the darker colour, reduced grain size and rare presence of K-feldspar porphyroclasts (SW of Juval transect). (b) Proto-mylonite with asymmetric K-feldspar porphyroclasts and incipient SCC' fabric showing a top-to-W sense of shear (S of Juval transect). (c) Mylonitic orthogneiss with ultra-mylonitic bands, recognizable from the dark grey-

black colour, extremely reduced grain size and quartz ribbons presence (SW of Juval transect). (d) Mylonitic paragneiss with an amphibolitic boudin (central part of Juval transect). (e) Mylonitic orthogneiss with quartz boudins (E of Schlanders transect). (f) Mylonitic orthogneiss with black, fine-grained ultra-mylonitic bands (E of Schlanders transect). (g) Protomylonitic orthogneiss (NW of Eyrts transect). (h) Phyllonite with quartz boudins (S of Eyrts transect). The image in the left corner shows the sample ERY-11, in which the calcite is clearly recognizable.

3.1.3. The Eyrts transect

The Eyrts transect covers the W part of the exposed VSZ, close to the Schling Normal Fault and Glurns Fault (Fig. 1 and 2) that crosscut the shear zone. The exposed part of the VSZ is here entirely developed again within the Ötztal polymetamorphic basement, chiefly made of granitoid orthogneiss. Protomylonites and mylonites are preserved only along the upper margin of the shear zone, whereas the remaining part, from 1300 down to 900 m.a.s.l. (meters above sea level), consists almost entirely of light grey to whitish phyllonites (Fig. 3g). The phyllonites' protolith is hardly identifiable in the field, but the widespread occurrence (see section 3.2) of K-feldspar suggests that mylonites and ultramylonites developed on pre-existing granitoid orthogneisses. Phyllonites are also exposed on the right side of the Vinschgau Valley (Fig. 2), NW of Prad am Stilfserjoch. This part of the VSZ was probably the best known to past authors, and its fault rocks were previously known as the "Eyrts phyllites". The occurrence of dispersed carbonates (Fig. 3h) within the phyllonites led some authors to suppose the occurrence of Permian-Triassic carbonate sediments entrapped within the VSZ (Schmid and Haas, 1989).

Mylonitic foliation dips NNW with a variable dip angle due to the occurrence of S-facing folds as described in the Schlanders transect (Fig. 2b). The mylonitic lineation, here mainly identified by iso-oriented sericite crystal on the foliation planes, is far less evident than in other sectors of the VSZ, but a WNW-ESE trend (Fig. 2b) is generally recognizable. The SPO of chlorite, white mica and quartz defines the mylonitic foliation. Extremely fine-grained quartz bands, a few millimetres thick, commonly occur (Fig. 3h). The light colour of the phyllonites turns frequently into a brownish aspect (Fig. 3h). This is due to the occurrence of dispersed fine-grained carbonates (mainly calcite and Fe-dolomite, Fig. 3h) that likely originated from secondary fluids circulating along the shear zone. Secondary carbonates have been also found within orthogneiss-derived mylonites of the Juval transect.

3.2. Microstructural analyses and kinematic vorticity of flow

Field structural analyses served as a base for sampling of the different structural facies recognized along the VSZ studied transects. Samples were collected (Supplementary Table 1) all along the three transects at regular distances in order to obtain a complete representation of the whole exposed shear zone.

Granitoid orthogneiss, the main protolith of the mylonites of the VSZ, does not represent the best opportunity for *PT* estimates. The scarce changes in the equilibrium mineral assemblage and the variation in the mineral chemistry of representative phases (white mica, biotite, K-feldspar and plagioclase) at greenschist and amphibolite facies conditions make difficult a precise estimate of pressure conditions and a qualitative, relative pressure determination can be estimated basing on the Si content of white mica. Maximum temperature of mylonites could instead be determined by the stability of chlorite vs. biotite along the mylonitic foliation and the dominant quartz recrystallization mechanism (Stipp et al., 2002).

In the Juval transect poorly deformed orthogneiss and proto- and mylonitic orthogneiss consist of plagioclase, quartz, K-feldspar, white mica, biotite and chlorite. Rutile, apatite, titanite and zircon occur as accessory phases. The regional foliation is made by the SPO of $Bt_1 + Wm_1$ (Zantedeschi, 1991; Bargossi et al., 2010). Rare relicts of pre-mylonitic Bt have been reported on the easternmost termination of the Partschinser orthogneiss body, outside the VSZ (Bargossi et al., 2010). The mylonitic foliation is defined by the SPO of $Wm_1 + Bt_1$, with white mica more abundant than biotite. Chlorite has been only rarely observed, mainly as an initial destabilization of biotite along rims of the Bt_2 grains. Bt_2 and Wm_2 overprinting the main foliation are observed in some samples (Fig. 4b).

In the poorly deformed orthogneiss, quartz is recrystallized mainly *via* bulging (BLG, Passchier & Trouw, 2005) recrystallization mechanism (Fig. 4a). Within proto- and mylonitic orthogneiss the dominant mechanism is subgrain rotation (SGR, Passchier and Trouw, 2005; Fig. 4b) recrystallization. A well-developed SCC' fabric (Fig. 5), together

with various groups of mica fish (group 1 to 5 of Passchier and Trouw, 2005; group 5 in Fig. 4c) and asymmetric K-feldspar porphyroclasts (Fig. 4d) point to a top-to-W shear sense, as already observed in the field.

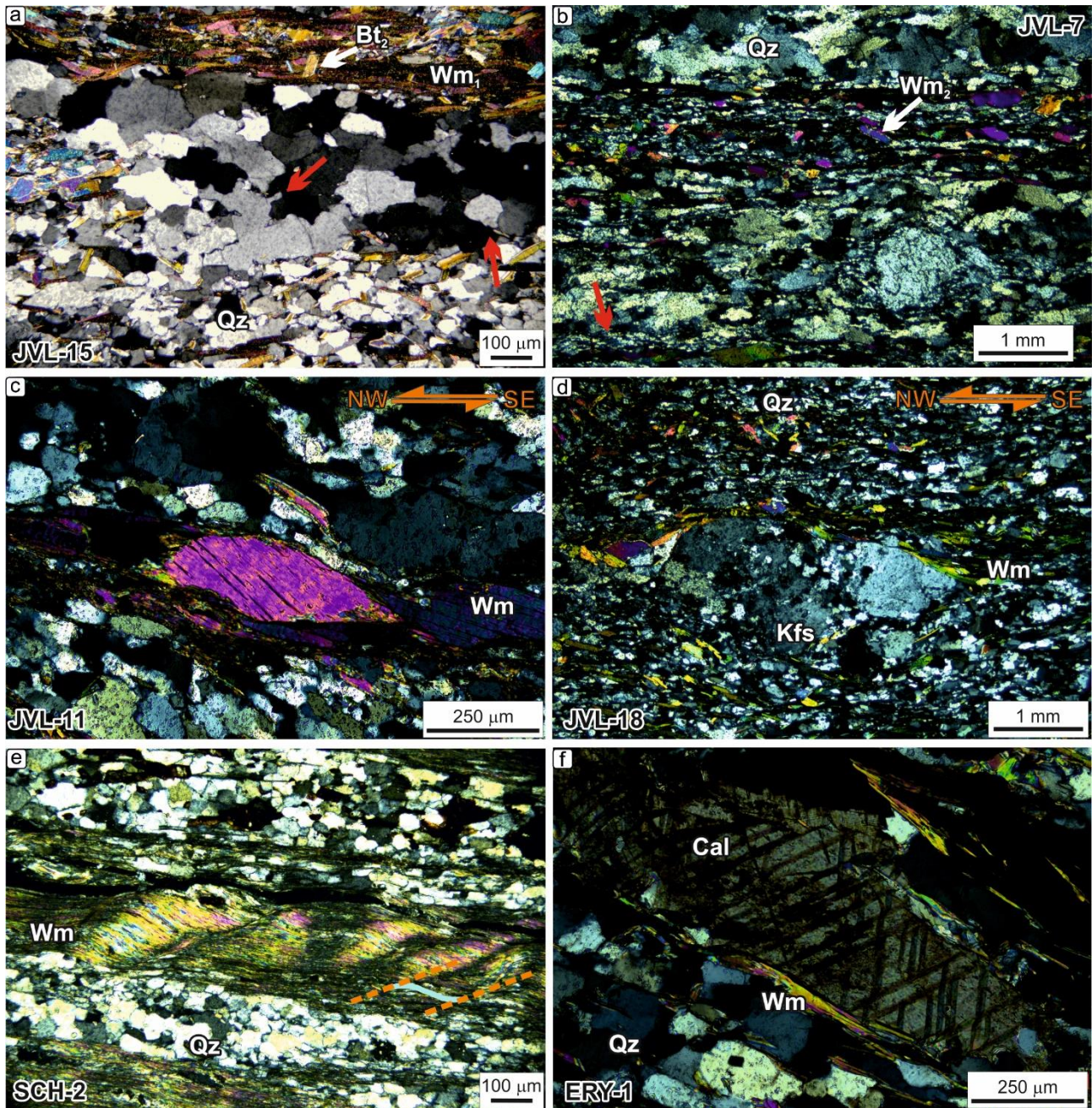


Figure 4: Representative photomicrographs from the VSZ, crossed polars. (a) Quartz recrystallized *via* bulging recrystallization mechanism (red arrows) in poorly deformed Partschinser orthogneiss. The white arrow points at Bt₂; (b) Quartz recrystallized *via* subgrain rotation recrystallization mechanism (red arrows) and static white mica (Wm₂, white arrow) growing on the main foliation (Wm₁) at high angle; close up on (c) group 5 mica fish according to the classification of Passchier and Trouw (2005) and (d) asymmetric K-feldspar porphyroclasts. (e) A well-developed crenulation cleavage in phyllonite, and (f) deformation twinning in calcite.

255

260

265

In the Schlanders transect, chlorite substitutes biotite along the mylonitic foliation, pointing to lower temperatures during shearing than in the Juval section. The syn-mylonitic foliation is defined here by the SPO of Ms_{III} + Chl. The complete mineralogy of mylonites consists of plagioclase, quartz, K-feldspar, white mica, chlorite and rare relicts of biotite. Apatite, rutile and zircon are usually present as accessory phases. Mylonites along the Schlanders transect are often seen to grade into phyllonites, with a strong decrease in grain size and a progressive increase of white mica with respect to chlorite. Within phyllonites, K-feldspar has been preserved only as relicts of 1-3 mm in size, with white mica becoming the major

mineral phase. The occurrence of fine-grained white mica domains characterize most of the phyllonites, often affected by a weak crenulation (Fig. 4e) in response of E-W trending S-facing folds, as previously described. Together with the increase of white mica abundance, also carbonates increase. They occur as calcite and Fe-calcite crystals, reaching about 5% in volume of the whole rock. Quartz in mylonites display textures compatible with SGR recrystallization, whereas BLG is the only recrystallization mechanism observed in phyllonites.

In the Eyr's transect, the westernmost and, following Schmid and Haas (1989), the shallowest transect of the VSZ, phyllonites completely substitute mylonites. The whole of the shear zone consists of light-grey to whitish extremely fine-grained phyllonites. Phyllosilicates domains reach up to 60% of the rock volume, with white mica as the major mineral phase. The abundance of calcite increase, reaching up to 10% in several outcrops. Calcite and Fe-calcite crystal show type 1 and type 2 deformation twinning (Ferrill et al., 2004; Fig. 4f). Quartz recrystallizes *via* BLG, no relicts of SGR and GBM textures have been observed in samples from the Eyr's transect. SCC' fabric, foliation fish, mica fish (group 3 and 4) and K-feldspar porphyroclasts occur as kinematic indicators, pointing to a top-to-W sense of shear.

280

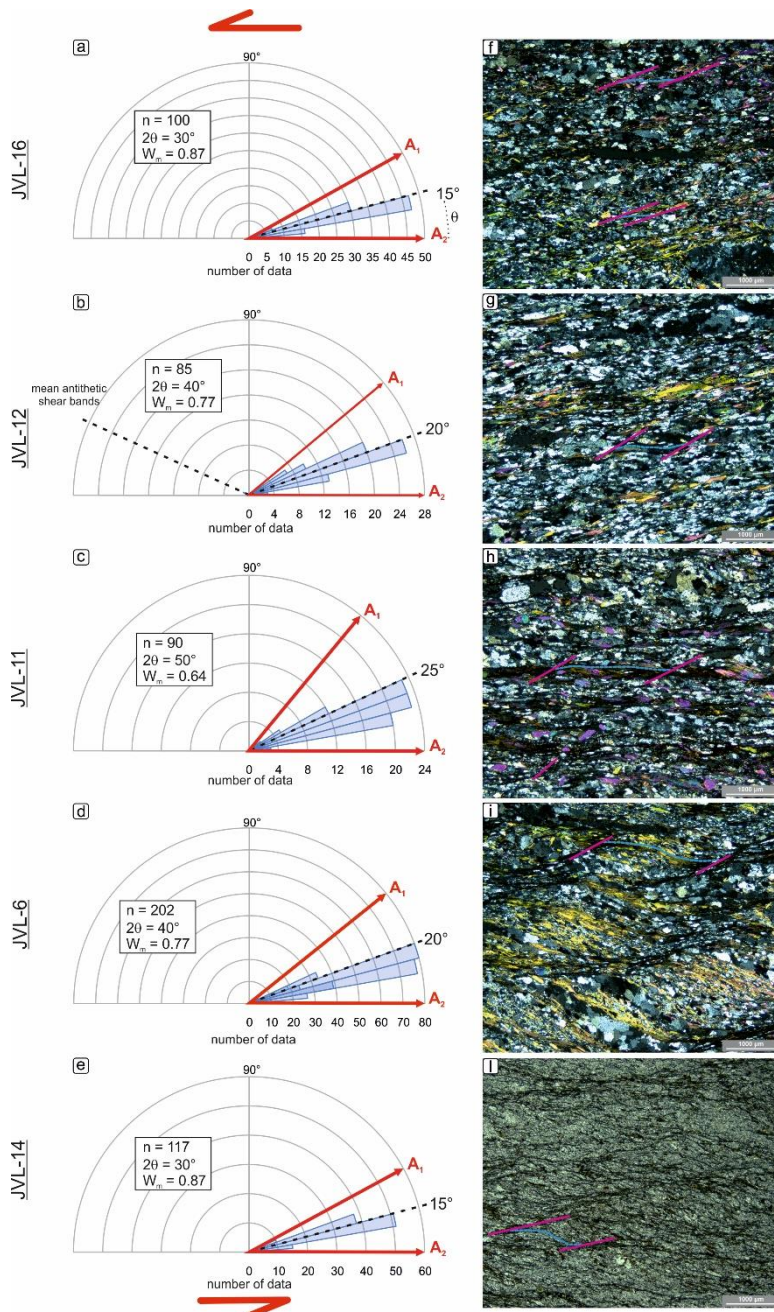


Figure 5: Vorticity estimates through SC' (a-e) and relative SC' fabric (f-l). Polar histograms used to derive the angle θ and to calculate kinematic vorticity with the SC' method (Kurz and Northrup, 2008) for samples JVL-16 (a), JVL-12 (b), JVL-11 (c), JVL-6 (d) and JVL-14 (e). C' shear bands are highlighted with violet lines and the main foliation S in dotted blue lines (f-l).

To define the type of flow within the VSZ, kinematic vorticity analyses were performed on five samples (JVL-16, JVL-12, JVL-11, JVL-6, JVL-14) collected along the Juval transect oriented perpendicular to the shear zone boundaries. The vorticity analysis were carried out on Juval samples, as they are suitable for vorticity estimates. Unfortunately, Schlanders and Eyr's mylonites are unsuitable for the application of any of the methods of vorticity estimates due to the lack of fabrics which allow applying vorticity estimate methods (e.g. shear bands fabric, porphyroclasts or oblique foliation in quartz). The analyses were performed on thin sections cut perpendicular to foliation and parallel to lineation (i.e. the XZ plane of the finite strain ellipsoid) using the C' shear band method (Kurz and Northrup, 2008), considering the mean value of the orientation of the synthetic shear bands following the interpretation of Gillam et al. (2013). Polar histograms used to derive the angle (2ν) between the apophyses A_1 and A_2 are reported in Figure 5. The C' shear band method reveals W_m ranging from 0.64 up to 0.87, corresponding to a variation in simple shear component of 46 - 68%, with the kinematic vorticity decreasing towards the core of the shear zone.

330 4. Petrochronology

4.1. Mineral chemistry

Electron microprobe analyses (EMPA) were carried out using a JEOL 8200 Super Probe EMP at the Dipartimento di Scienze della Terra "A. Desio", Università degli Studi di Milano. Quantitative chemical analyses were performed on carbon-coated petrographic thin sections. Data acquisition was performed using an accelerating voltage of 15 kV, a beam current of 5 nA with a spot size of 1 μ m. Natural silicates and oxides were used as standards. White mica and biotite analyses were recalculated as atoms per formula unit (apfu) based on 11 oxygens.

Quantitative chemical analyses were performed on a non-mylonitic orthogneiss sample (JVL-15), on mylonitic orthogneiss samples (JVL-1, JVL-7, JVL-13, SCH-4) and on a phyllonite sample (ERY-11), with a total of about 100 points. Chemical analyses are reported in Figure 6 and Supplementary Table 2. Both first and second generation of micas were analysed: the microstructurally older white mica and biotite generation forming the main mylonitic foliation (hereafter W_{m1} and B_{t1}) and the following, static, white mica and biotite generation overprinting the preceding one (hereafter W_{m2} and B_{t2}).

4.1.1. White mica

Considering all six samples, some compositional variations around the muscovite-celadonite join can be observed, with Si ranging between 3.1 and 3.4 apfu and Al ranging between 2.17 and 2.71 apfu (Fig. Xa). White mica in ERY-11 is characterised by the highest Al/Si ratios, while the other samples show a gradually decreasing Al/Si ratios, with JVL-7 and SCH-4 being the lowest (Fig. 6a). White mica in JVL-1, JVL-7, JVL-13 and JVL-15 samples is characterised by a negative correlation between Al and Si content (Fig. 6a), ranging from Si content between 3.14 and 3.35 apfu and Al content between 2.17 and 2.55 apfu. White mica from sample JVL-7 displays a compositional cluster characterised by high Si content (3.30-3.34 apfu) and low Al content (2.17-2.22 apfu), whereas white mica from sample JVL-15 shows an opposite cluster with low Si (3.17-3.20 apfu) and high Al (2.46-2.49 apfu) content (Fig. 6a). No variations in Al and Si contents have been detected between first- and second-generation white mica (Ms_1 and Ms_2 , respectively).

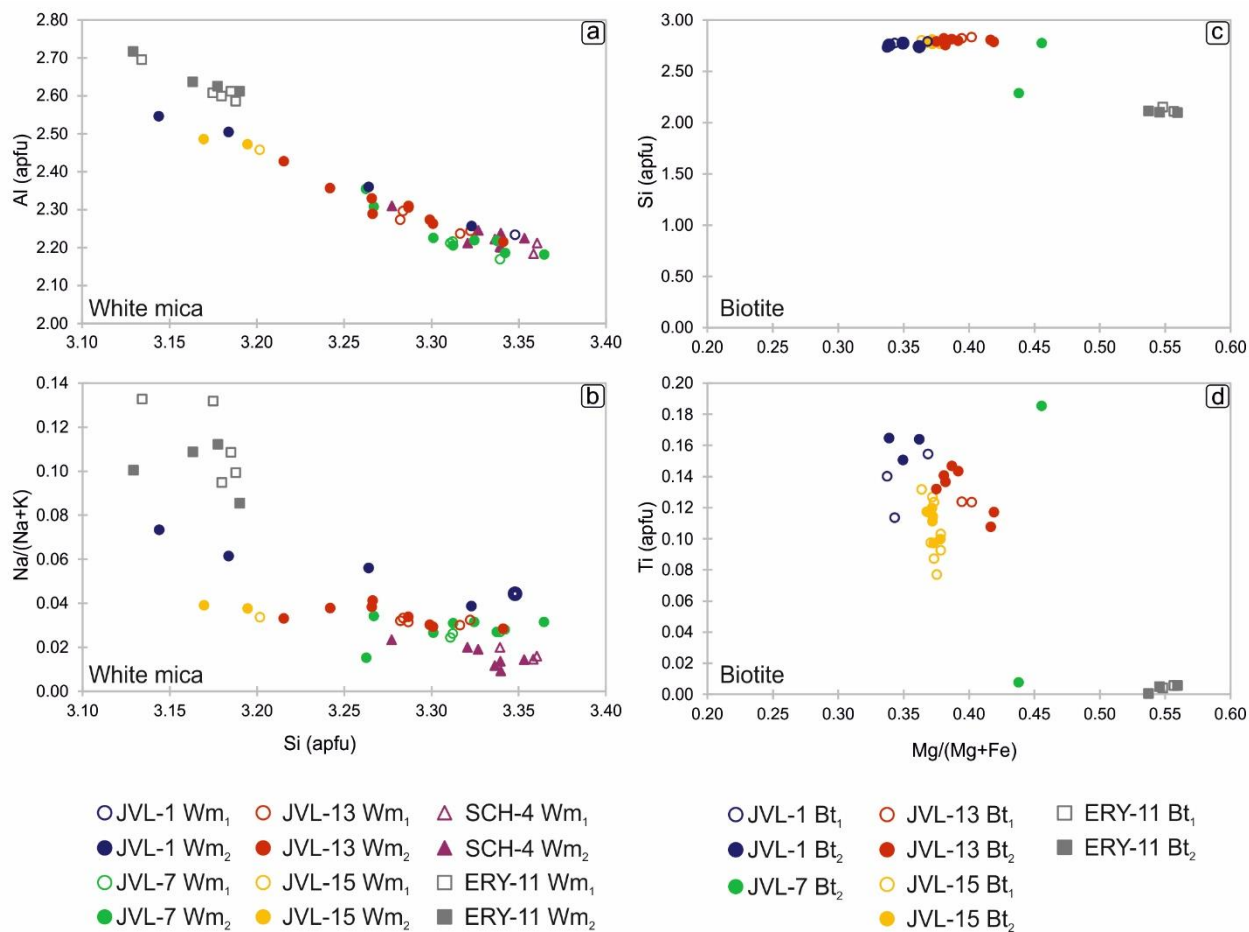
The Na/(Na+K) ratio (Fig. 6b, Guidotti and Sassi, 2002) of white mica in sample ERY-11 is higher (0.09-0.13) than in sample SCH-4 (0.01-0.02) and in samples JVL-1, JVL-7, JVL-13 and JVL-15 (0.02-0.07). No variations of the Na/(Na+K) ratio were observed on W_{m1} and W_{m2} . White mica in JVL-1, JVL-7, JVL-13 and JVL-15 samples show a homogenous distribution of the Na/(Na+K) ratio (0.02-0.07), with Si content ranging between 3.14 and 3.34 apfu (Fig. 6b).

4.1.2. Biotite

Analyses were performed on biotite from five samples, since it was absent from sample SCH-4. In the sample ERY-11 the X_{Mg} ratio ranges between 0.54 and 0.56 (Fig. 6c-d), whereas X_{Mg} of the other samples shows a cluster at lower values (0.34-0.46). As in the case of white mica analyses, no significant chemical variations have been observed between the two biotite generations (B_{t1} and B_{t2}).

365 The Si content of biotite in sample ERY-11 is homogenous, while in samples JVL-1, JVL-7, JVL-13 and JVL-15 it shows a cluster characterised by Si content between 2.74 and 2.83 apfu (Fig. 6c). The Ti content in biotite from samples JVL-1, JVL-7, JVL-13 and JVL-15 is clustered at values between 0.08 and 0.17 apfu (Fig. 6d), apart from a biotite-2 from sample JVL-7 which shows a remarkably lower value (0.01 apfu), like sample ERY-11 (0.001-0.006 apfu).

370 The K content (Suppl. Table 2) reveals that in sample ERY-11, all the spot analyses yielded low, sub-stoichiometric K in Bt₁ and Bt₂. These values, very close to the detection limit (ca. 0.006-0.010 apfu) pertain to chlorite, as also supported by the matching element sums below 96% for these analyses (Suppl. Table 2). Biotite from samples JVL-1, JVL-7, JVL-13 and JVL-15 is characterised by K content of 0.93-1.00 apfu, except for a biotite-2 from sample JVL-7, which again shows low K content (0.02 apfu). As in the case of sample ERY-11, the low K content and the element sums (c. 89%; Suppl. Table 2) confirm the presence of chlorite in the sample.



375 **Figure 6: EPMA results showing compositional variation in white mica (a–b) and biotite (c–d).**

4.2. ⁴⁰Ar/³⁹Ar geochronological constraints on the VSZ activity

380 White mica and biotite used for ⁴⁰Ar/³⁹Ar geochronology were obtained from rock samples: JVL-1, JVL-7, JVL-13, JVL-15, SCH-1, SCH-4, SCH-5, ERY-3, ERY-8 and ERY-11. The mineral separation was performed at the Dipartimento di Scienze dell'Ambiente e della Terra, Università degli Studi di Milano - Bicocca. Rock samples were crushed and sieved, then Wm₁ and Bt₁ in the 125-500 μm fraction were enriched by magnetic techniques and subsequently purified by hand-picking. Mica separates were cleaned and rinsed in pure deionized water by a two steps procedure in ultrasonic baths.

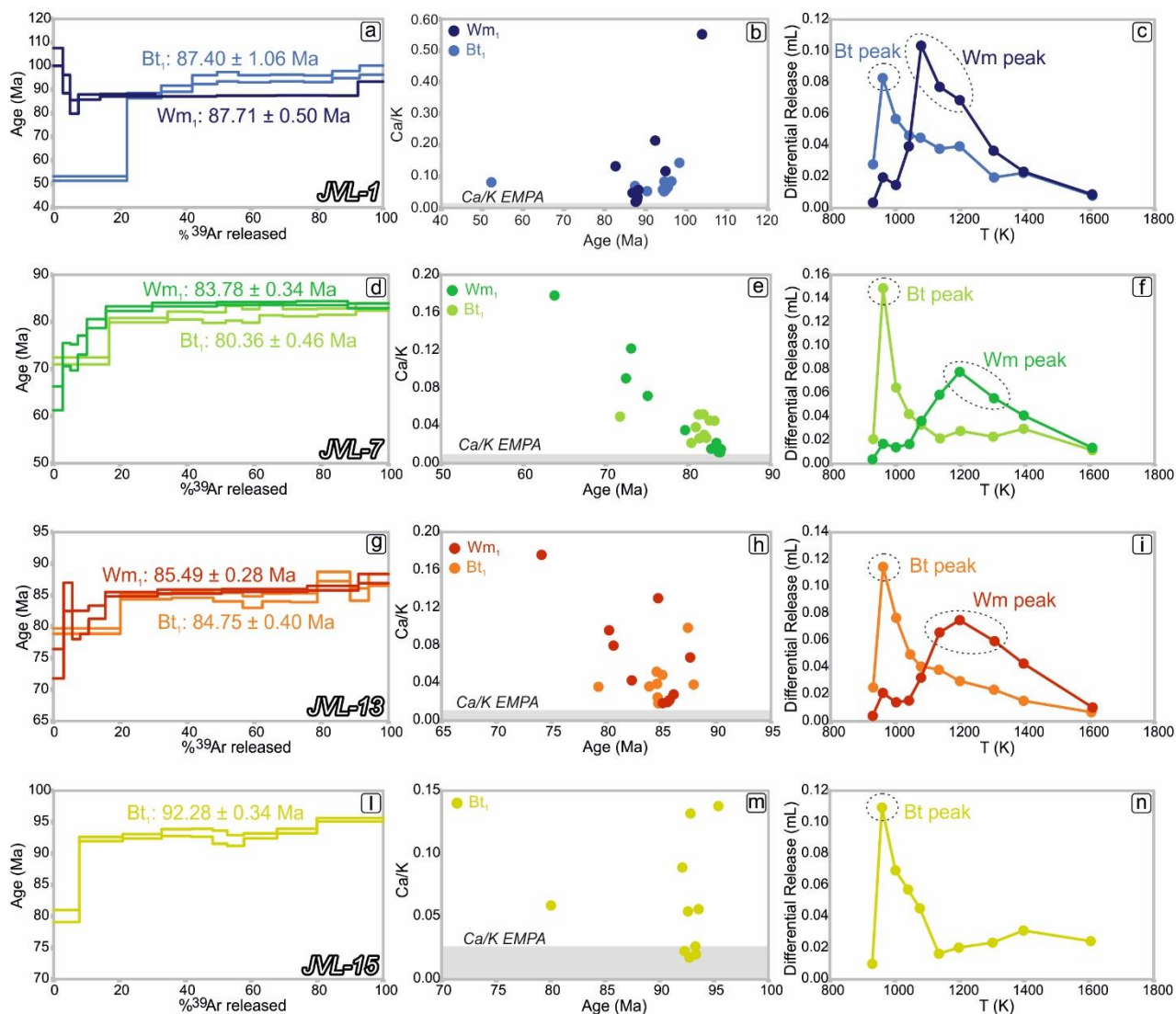
385 Mica samples were irradiated in the McMaster University Research Reactor (Hamilton, CA), carefully avoiding Cd shielding. ⁴⁰Ar/³⁹Ar step-heating analyses were carried out using a double-vacuum resistance furnace attached to a NuInstruments Noblesse rare gas mass spectrometer at the Dipartimento di Scienze dell'Ambiente e della Terra, Università degli Studi di Milano - Bicocca. The irradiation monitor was McClure Mountain hornblende (MMhb) with an assumed age of 523.98 ± 0.12 Ma (Schoene and Bowring, 2006). The decay constants were those of Steiger and Jäger

390 (1977). Step heating experiments were conducted following the analytical protocols of Montemagni and Villa (2021).
 This approach evaluates and integrates the information deriving from the age spectra, the correlation diagram (i.e. Ca/K
 vs. age) and the differential release plot (i.e. T vs. differential release). The obtained ages are therefore isochemical ages:
 the step used for the age calculation are those with lowest and homogeneous Ca/K ratios which correspond to ^{39}Ar highest
 release and % of ^{39}Ar . All $^{40}\text{Ar}/^{39}\text{Ar}$ data are reported in Supplementary Table 3.

395

4.2.1. The Juval transect

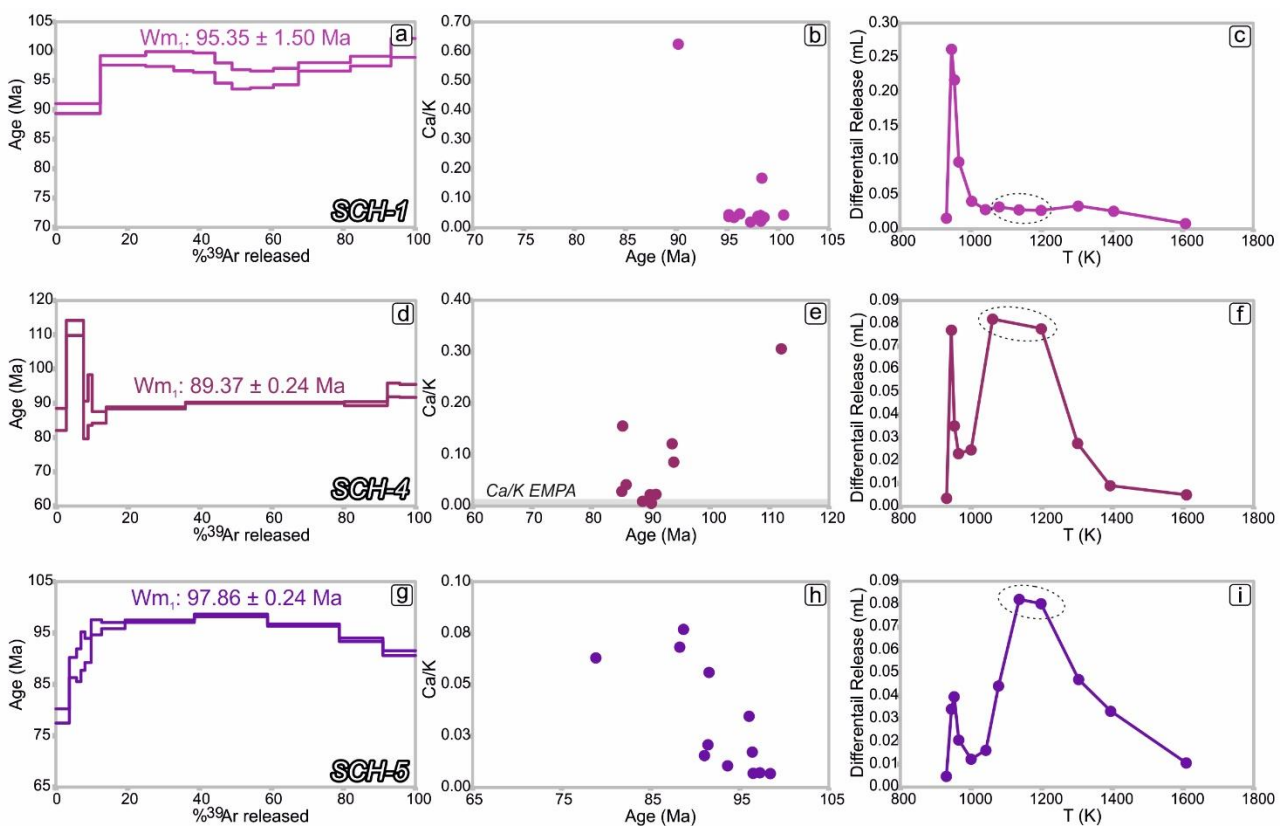
The age spectrum, the correlation diagram (Ca/K vs age) and the Differential Release Plots (DRP) for white mica display
 similar features (Fig. 7). The ^{39}Ar degassing peaks in the DRP (occurring at temperature ranging in the ca. 1080 – 1300
 K interval) correspond to the flat part of the spectrum and the lowest Ca/K values, as imposed by white mica
 stoichiometry, which should be Ca-free. The heating steps showing high Ca/K and high Cl/K ratios (derived from the
 400 measured $^{37}\text{Ar}/^{39}\text{Ar}$ and $^{38}\text{Ar}/^{39}\text{Ar}$), monitor the degassing of Ca-rich alteration phases and have been disregarded in the
 age calculation. At higher temperatures pertaining to white mica or biotite degassing, the Ca/K and Cl/K reach a minimum.
 Biotite gas release patterns behave likewise, whereby the ^{39}Ar -release peak occurs at lower temperature (ca. 960 K; Fig.
 7 c-f-i-n), as extensively documented for Himalayan mylonites by Montemagni and Villa (2021) and Alpine ones in
 405 Montemagni and Zanchetta (2022). The age of mylonitic foliation on biotite, constraining the VSZ activity, is: 87.40 ± 1.06 Ma
 (JVL-1; Fig. 7a), 80.36 ± 0.46 Ma (JVL-7; Fig. 7d), 84.75 ± 0.40 Ma (JVL-13; Fig. 7g) and 92.28 ± 0.34 Ma
 (JVL-15; Fig. 7l).



410 **Figure 7:** $^{40}\text{Ar}/^{39}\text{Ar}$ age spectra, Ca/K vs. age diagrams and Differential Release Plots for Juval samples JVL-1 (a–c), JVL-7 (d–f), JVL-13 (g–i) and JVL-15 (l–n). The dotted circles in the T vs. differential release plots (c, f, i, n) indicate the degassing steps selected for the age calculation.

415 **4.2.2. The Schlanders transect**

The ^{39}Ar release patterns of the three white mica samples SCH-1, SCH-4 and SCH-5 (Fig. 8) are different from those of Juval. All three Schlanders samples show a bimodal ^{39}Ar peak pattern: one release around 940 K, typical of chlorite (see Montemagni and Villa, 2021), and one around 1050 - 1150 K, typical of white mica. In SCH-4 and SCH-5 the white mica release peak corresponds to the lowest Ca/K ratios, i.e. the flat part of the spectra. In SCH-1 the white mica release peak is not very evident but the three steps between 1080 and 1200 K correspond to low and homogenous Ca/K ratios, coherent with the Ar release in SCH-4 and SCH-5. The age of mylonitic foliation has been constrained at 95.35 ± 1.50 Ma (SCH-1; Fig. 8a), 89.37 ± 0.24 Ma (SCH-4; Fig. 8d) and 97.86 ± 0.24 Ma (SCH-5; Fig. 8g).



425 **Figure 8:** $^{40}\text{Ar}/^{39}\text{Ar}$ age spectra, Ca/K vs. age diagrams and Differential Release Plots for Schlanders samples SCH-1 (a–c), SCH-4 (d–f) and SCH-5 (g–i). The dotted circles in the T vs. differential release plots (c, f, i) indicate the degassing steps selected for the age calculation.

430 **4.2.3. The Eyrs transect**

The phyllonites (ERY-3 and ERY-8) contain dispersed carbonates, evidence of massive fluid circulation (Fig. 3h). Moreover, due to the lower strain rate and/or lower temperature, the micas did not fully recrystallize during the Cretaceous faulting and give meaningless mixed ages with substantial Ar inheritance and white mica ages are geologically meaningless (Fig. 9 a-d). The age of mylonitic foliation has been constrained to be 92.58 ± 1.56 Ma (ERY-11; Fig. 9g).

435

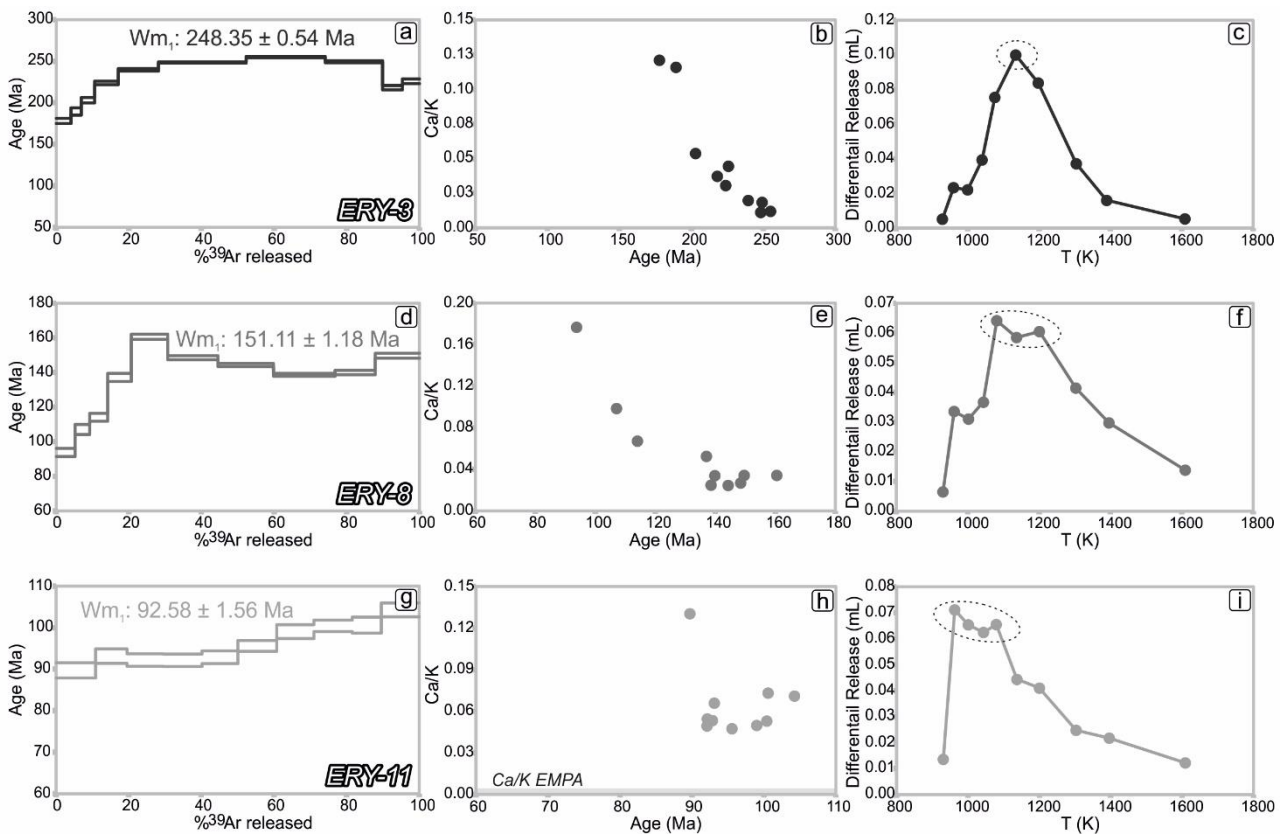


Figure 9: $^{40}\text{Ar}/^{39}\text{Ar}$ age spectra, Ca/K vs. age diagrams and Differential Release Plots for Eyr's samples ERY-3 (a–c), ERY-8 (d–f) and ERY-11 (g–i). The dotted circles in the T vs. differential release plots (c, f, i) indicate the degassing steps selected for the age calculation.

440

5. Discussion

5.1. Kinematic and chronological evolution of the VSZ

445

Although the Vinschgau Shear Zone (VSZ) is likely the largest thrust-sense shear zone exposed in the Alps, no age constraints existed on the shearing activity of this huge intra-Austroalpine thrust, with its Late Cretaceous age only inferred on the base of indirect evidence (Schmid and Haas, 1989) and a single Rb-Sr whole rock age of a deformed pegmatite (Thöni, 1986). Our $^{40}\text{Ar}/^{39}\text{Ar}$ data are the first attempt to constrain the time interval of activity of the VSZ, combining geochronological results obtained across the shear zone and along its dip direction.

450

The evolution of shear zones has been deeply investigated in terms of spatial variation especially concerning their length and thickness (Hull, 1988; Mitra, 1992; Means, 1995; Vitale and Mazzoli, 2008, 2010; Fossen, 2010; Fossen and Cavalcante, 2017). This effort was aimed at defining the parameters that may influence the evolution of one type of shear zone with respect to another one. If the growth in length of a shear zone is essentially due to linkage of different branches forming a composite system of shear zones (Fossen and Cavalcante, 2017), the growth in thickness may be influenced by different mechanisms. Four ideal models of shear zone evolution have been proposed and discriminated based on shear strain gradient, kinematic vorticity and plane or triaxial strain (Vitale and Mazzoli, 2008; Fossen and Cavalcante, 2017).

455

Processes of strain hardening or strain softening promote the thickening and the thinning of the shear zone, respectively *type-1* or *type-2* models. In the *type-1* model, the deformation concentrates in the margins of the shear zone, leaving inactive the inner portion. On the contrary, in the *type-2* model the deformation shifts and concentrates in the inner portion of the shear zone as strain accumulates, leaving the margins inactive. In addition, *type-3* model is related to a strain weakening process, even if its active thickness remains constant with time. *Type-4* model expands in thickness but, unlike *type-1*, all the thickness remains active through time. According to the several models proposed for shear zone evolution (Fossen and Cavalcante, 2017 with references), the VSZ followed a *type-2* evolutionary model, with increasing

460

465 cumulative shear strain from margins to the core of the shear zone (Fig. 10). This pattern of shear strain distribution is demonstrated for the VSZ by the occurrence of ultramylonites at the core of the Juval transect (Fig. 10), whereas protomylonites derived from the Partschinser orthogneiss are preserved only at the margins. The kinematic vorticity of flow follows the same symmetric distribution, with W_m that increases from the rims to the core (ca. 0.64 at margins and ca. 0.87 at the core, Fig. 10). The patterns displayed by the shear strain points to a strain-softening behavior of the shear zone (e.g. Vitale and Mazzoli, 2008). At the microscale, the processes that may cause strain softening are: (i) 470 recrystallization during shearing, especially when associated with subgrain rotation recrystallization mechanism (Passchier and Trouw, 2005), which leads to formation of new grains with lower dislocation density that results in a deformation at lower differential stress; (ii) shear bands fabric formation (Fig. 5), as shear bands imply local grain-size reduction, a mechanism which is invoked in low-to-medium mylonitization to promote strain weakening (Fossen and Cavalcante, 2017 and references therein). Lattice preferred orientation (Fig. 4) may also weaken the rheology as 475 recrystallized or newly formed minerals, mainly micas and quartz, have intracrystalline slip planes aligned in the shear direction, resulting in favorable motion of dislocations with continuous dynamic recrystallization also at low differential stress (Passchier and Trouw, 2005 with references).

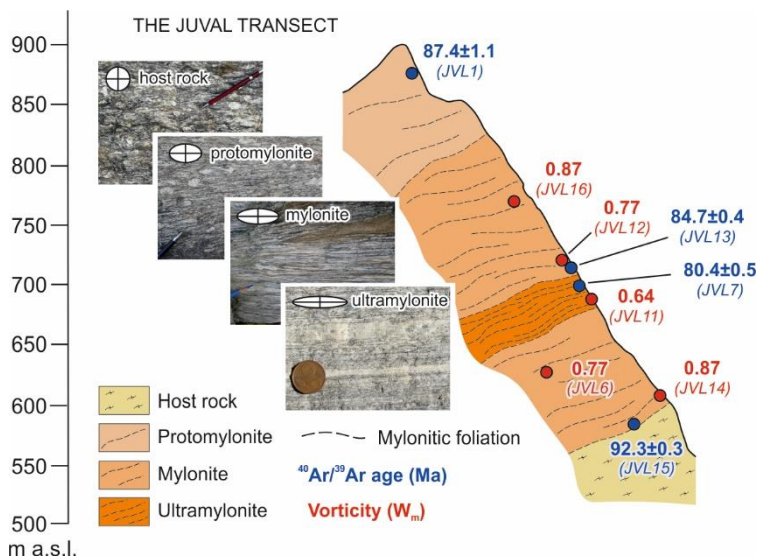


Figure 10: schematic cross section of Juval transect showing the occurrence of protomylonites, mylonites and ultramylonites developed along the strain gradient from rim to core of the shear zone, with $^{40}\text{Ar}/^{39}\text{Ar}$ age (in blue) and kinematic vorticity number (in red). Samples not on the profile have been projected along the strike of the mylonitic foliation.

495 The VSZ deepens from W to E, as suggested by previous workers (Schmid and Haas, 1989) and confirmed by the present data, with white mica-chlorite phyllonites overprinting white mica-biotite mylonites in the western part of the shear zone. Broadly, the $^{40}\text{Ar}/^{39}\text{Ar}$ ages rejuvenate from W to E, opposite to the transport direction and consequent exhumation of the Austroalpine units in the hanging wall. This age pattern points for younger ages of shearing in the E (i.e. Juval area) where deeper portions were still being deformed (Fig. 11), while in the W the shear zone was already at shallow crustal depths. 500 Beyond the deformational path of the VSZ, which clearly follows a strain softening *type-2* shear zone evolution model, the novelty of our work is the integration of microstructural and kinematic analyses with age profiling of the shear zone along its transport direction, along depth, and across strike (Fig. 11). The obtained age pattern allows the reconstruction of a time-resolved evolution of the shear zone during its progressive activity and exhumation. The $^{40}\text{Ar}/^{39}\text{Ar}$ ages recorded by micas in the Schlanders and Juval transects reveal a clear younging trend from the margin 505 to the inner zone of the shear zone (Figs. 7, 8 and 11). This trend of younging mica ages is paralleled by increasing cumulative shear strain and decreasing simple shear component (Fig. 11). The correlation between ages and deformation suggests a progressive migration of deformation towards the inner portion of the VSZ, with the margin becoming inactive (as testified by older mylonite ages ≥ 97 Ma), while deformation concentrates in the middle of the shear zone where micas show younger ages down to 80 Ma.

510

5.2. The VSZ in an evolving orogenic wedge

The evolution of the Eo-Alpine orogenic wedge of the Eastern Alps is generally related to the closure of the Meliata-Hallstatt ocean, located in an intra-Austroalpine position (e.g. Schmid et al., 2004), or separating the former Austroalpine and Southalpine domain (e.g. Neubauer et al., 2000). Other interpretations consider instead the possibility that the entire Austroalpine orogenic wedge formed in the Late Cretaceous in a pre-collisional setting (Zanchetta et al., 2012, 2015). Irrespective of the geodynamic scenario of the Eo-Alpine orogen in the Eastern Alps, the VSZ acted as a crustal-scale shear zone promoting nappe stacking and exhumation within an orogenic wedge chiefly made of continent-derived tectonic units. The ages of shearing along the VSZ indicate that the shear zone was already active at 97 Ma (Fig. 7, Fig. 8 and Fig. 11), at least 7-8 Ma before the pressure peak recorded by the Texel eclogites and the amphibolitic peak in the Schneeberg unit. The ages of the VSZ in the Schlanders transects overlap with published/available ages related to the peak of Alpine metamorphism in the Ötztal basement, suggesting that thrusting within the Austroalpine domain started where units in the hanging wall of the VSZ had already reached (Ötztal) or were close to the metamorphic peak (Texel and Schneeberg units). These ages overlap between shearing and metamorphic peak is explained by a rapid exhumation of these HP rocks *via* thrusting in the Eo-alpine orogenic wedge. Handy et al. (2010) argued that the Eo-alpine orogen, in the time span 118-84 Ma, was subjected to intracontinental subduction and basement nappe stacking, whose evidence is the E-W trending belt of Late Cretaceous, HP rocks of the Koralpe-Wölz nappe complex (Schmid et al., 2004; Thöni et al., 2008), to which the Texel and Schneeberg units belong. The exhumation of these HP rocks was both westward and northward (Handy et al., 2010).

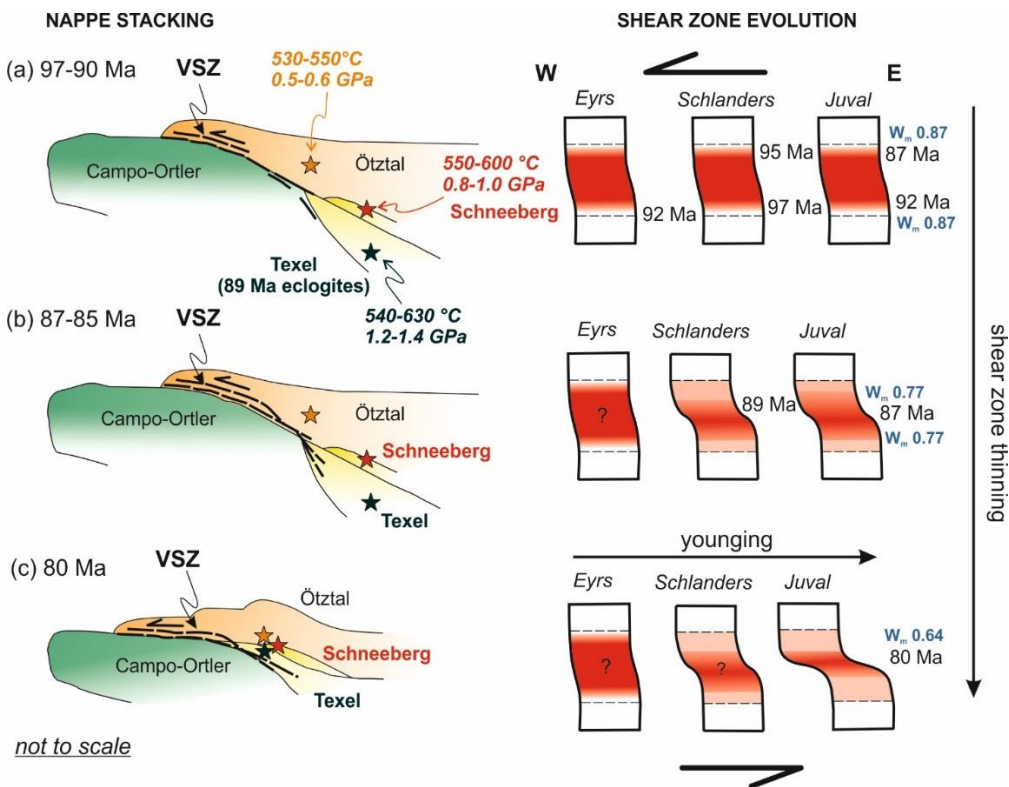


Figure 11: Evolution of the Vinschgau Shear Zone in the orogenic Eo-alpine wedge during the Late Cretaceous. Activation of the VSZ (a) in the time span 97-90 Ma affecting the Ötztal unit, (b) in 87-85 Ma the VSZ affected also the Texel unit and (c) during the late stage of shearing exhumed the Texel and Schneeberg units to Ötztal PT conditions. In (a) the PT conditions for Ötztal, Texel and Schneeberg units are reported. The dashed lines represent the thickness and length of the shear zone through time. The evolution of the VSZ in the studied transects in term of ages, cumulative shear strain and kinematic vorticity is also shown.

The W/SW-directed Late Cretaceous thrusting (Eisbacher and Brandner, 1996; Ratschbacher, 1986; Schmid and Haas, 1989; Viola et al., 2003; Handy et al., 2010) and consequent nappe stacking under pressure-dominated, amphibolite to

540 greenschist facies conditions, is unusual, if compared to major N/NW-directed direction of transport for other sector of Alps. This scenario has been explained through a complex microplate configuration at 94 Ma, which necessarily invokes the eastward faster accommodation of the Iberia microplate with respect to the Adria microplate, also moving eastward with respect to Europa, but at lower rates (Handy et al., 2010).

545 The age of the pressure metamorphic peak within HP units has been reported between 95 and 89 Ma (Thöni, 2002; Habler et al., 2006; Miller et al., 2005; Thöni et al., 2008; Janák et al., 2009; Zanchetta et al., 2013), with partially overlapping ages related to their rapid exhumation (e.g. Fügenschuh et al., 1997; Sölva et al., 2005).

550 As the Texel and the Ötztal units are now in tectonic contact at the eastern termination of the VSZ, at least 20 km of vertical exhumation of the Texel unit should have been accommodated along the VSZ, considering the difference in peak metamorphic pressure recorded by the two units (Fig. 11a): 1.2-1.4 GPa for the Texel unit (Habler et al., 2006) and 0.5-0.6 GPa for the Ötztal basement (Purtscheller and Rammlmair, 1982). Considering a lithostatic pressure gradient of 0.03 GPa/km and a consequent difference in terms of pressure of 0.6 GPa between the Ötztal and the Texel unit, such vertical displacement corresponds to a minimum of about 40 km along the shear zone, taking into account a dip of about 30°, which is typical of thrust-sense shear zone active through crustal depths controlling the exhumation of high-grade units in their hanging wall (e.g. Jamieson et al., 2004). The amount of E-W shortening within the Austroalpine basement nappes has been estimated to be ≥ 100 –150 km (Manatschal and Bernoulli, 1999; Schmid et al., 2020).

555 The VSZ yields ages in the range of 80 Ma (the youngest age at the inner portion of Juval transect) and 97 Ma (the oldest age in the Schlander area) almost coeval with the peak metamorphic age in the Ötztal and Texel units at ca. 85-90 Ma (Zanchetta et al., 2013, Fig. 11). Hence, we argue that the VSZ has been active at least for 17 Ma, promoting the rapid exhumation of the Texel eclogite in the Late Cretaceous. Syn-shearing exhumation of the Texel and Schneeberg units continued at least up to 76 Ma, as testified by the age of greenschist facies mylonites along shear zones within these two units (Sölva et al., 2005). This scenario was depicted also by Handy et al. (2010), who suggested a rapid exhumation of the Koralpe-Wölz units during the Cenomanian - Santonian (ca. 94-84 Ma) when the Gosau Group (syn- to post-orogenic clastic sediments sometimes deposited in intra-orogenic extensional basins) sealed thrusts in the Austroalpine basement and in the Northern Calcareous Alps.

560 Exhumation models for crystalline rocks have been extensively proposed, modeled and tested for the Himalayan orogen, where the exhumation of the metamorphic core of the belt was matter of debate in the literature (e.g. Montomoli et al., 2015; Carosi et al., 2018; Montemagni, 2020). Regardless the specific model, the scientific community agrees that exhumation in the Himalayas has been driven by two opposite shear zone bounding the crystalline core: a normal-sense at its top and a thrust-sense shear zone at its bottom, respectively (e.g. Godin et al., 2006; Montomoli et al., 2013 for reviews). Based on structural and geochronological data, a similar model was also proposed for the type locality eclogites in the Saualpe region (Wiesinger et al., 2006). A recent study (Schulz and Krause, 2021) documented the younger age in amphibolite-grade footwall units underlying the eclogite-bearing unit.

565 In this perspective, we argue that the VSZ played a key role in the exhumation of HP rocks in the Eastern Alps, and we can speculate that the units containing HP rocks have been exhumed by a (non-necessarily coeval) shearing of a thrust-sense shear zone at the base and a normal-sense shear zone at the top of the orogenic wedge, i.e. above the Ötztal-Stubai complex. Considering the jump in the metamorphic grade and age of metamorphism between the underlying Eo-Alpine Ötztal-Stubai complex (garnet amphibolites facies) and the quartz-phyllites (ca. 350 °C of peak temperature, Lünsdorf et al., 2012) with a pre-Permian metamorphic age (Rockenschaub et al., 2003) of the Steinach Nappe, the shear zone at the base of this nappe could be a valuable candidate for the normal-sense shear zone that together with the VSZ controlled the exhumation of the Ötztal-Stubai-Schneeberg high-pressure complex.

575 Beside the geodynamic interpretation, the presented data indicate that the VSZ had a long-lasting evolution of at least 17 Myrs. The minimum accommodated displacement of ca. 40 km implies a displacement rate of 2-2.5 mm/yr that is significantly higher than values reported in Vitale and Mazzoli (2008) that are of 0.10 mm/yr for thinning shear zone (*type-2*). The accommodated displacement of the VSZ is coherent with slip rate values of ca. 10 mm/yr reported by 580 Stübner et al. (2013) for an intrabasement normal sense shear zone in the Pamir plateau. The exhumation continued

rapidly as suggested by thermochronological data in the eastern Ötztal-Stubai complex unit where cooling below 60 °C at 60 Ma has been reported (Fügenschuh et al., 1997).

6. Conclusions

590 The VSZ is one of the prominent intra-basement thrust-sense shear zone developed in the Alps, promoting the exhumation of HP rocks within the Eo-Alpine orogenic wedge.

Our approach fully constrains its kinematic and temporal evolution:

- (i) Cumulative shear strain and kinematic vorticity values reveal an evolution compatible with a *type-2* thinning shear zone.
- 595 (ii) ⁴⁰Ar/³⁹Ar geochronology defines the shearing activity to be comprised between 97 and 80 Ma, resulting in a long-lasting deformation history.
- (iii) The novelty of our work is the combination of microstructural and kinematic analyses with age profiling of the shear zone both along its transport direction and across strike.

600

Author contribution. SZ, AZ and CM designed the study, CM and MR carried it out. The paper was prepared by CM and SZ and revised by AZ – with the contribution of all co-authors. All authors participated in fieldwork and in the various scientific discussions.

605 *Competing interests.* None of the authors has any competing interests.

Acknowledgements. This research was funded by MUR through the PRIN project FAST, 2021-NAZ-0299 (CUP: J33C22000170001), and by the CARG project of the Autonomous Province of Bozen – South Tyrol.

610 We warmly thank the reviewers Paolo Conti and Frantz Neubauer for their careful and significant comments that improved the paper and the Yang Chu for the editorial handling of the manuscript. We are also grateful to Hannah Pomella for corrections of the German toponyms and discussion about the Vinschgau geology that helped us to clarify some aspects. We thank A. Risplendente (Università degli Studi di Milano) for his support during the electron microprobe analyses and V. Barberini (Università degli Studi di Milano - Bicocca) for the maintenance of the mass spectrometer.

615

References

Bargossi, G. M., Bove, G., Cucato, M., Gregnanin, A., Morelli, C., Moretti, A., Poli, S., Zanchetta, S., and Zanchi, A.: Note illustrative della Carta Geologica d'Italia—Merano foglio 013, Servizio Geologica d'Italia — ISPRA, 2010.

620 Brunel, M.: Quartz fabrics in shear-zone mylonites: evidence for a major imprint due to late strain increments, *Tectonophysics*, 64(3-4), T33-T44, 1980.

Caby, R., Pêcher, A., and Le Fort, P.: Le grand chevauchement central himalayen: Nouvelles données sur le métamorphisme inverse à la base de la Dalle du Tibet, *Rev. Géol. Dynam. Géograph. Phys.*, 24, 89–100, 1983.

Carosi, R., Montomoli, C., and Iaccarino, S.: 20 years of geological mapping of the metamorphic core across Central and Eastern Himalayas. *Earth-Sci. Rev.*, 177, 124-138, 2018.

625 Conti, P.: La Falda Austroalpina dell'Ortles e l'evoluzione tettonica delle Dolomiti dell'Engadina (Svizzera-Italia), *Memorie Descrittive della Carta Geologica D'Italia*, Servizio Geologico d'Italia, Roma, 53, 102 pp., 1997.

D'Adda, P. and Zanchetta, S.: Geological-structural map of the Orobic and Porcile thrust junction, central Southern Alps (N Italy), *J. Maps*, 11(1), 25–38, 2015.

630 Eisbacher, G. H., and Brandner, R.: Superposed fold-thrust structures and high-angle faults, Northwestern Calcareous Alps, Austria, *Eclogae Geol. Helv.*, 89 (1), 553–571, 1996.

Ferrill, D. A., Morris, A. P., Evans, M. A., Burkhard, M., Groshong Jr, R. H., and Onasch, C. M.: Calcite twin morphology: a low-temperature deformation geothermometer, *J. Struct. Geol.*, 26, 1521-1529, 2004.

- Fossen, H.: Structural geology, Cambridge University Press, 2010.
- 635 Fossen, H. and Cavalcante, G. C. G.: Shear zones—A review, *Earth Sci. Rev.*, 171, 434–455, <https://doi.org/10.1016/j.earscirev.2017.05.002>, 2017.
- Froitzheim, N., Conti, P., and van Daalen, M.: Late Cretaceous, synorogenic, low-angle normal faulting along the Schlinig fault (Switzerland, Italy, Austria) and its significance for the tectonics of the Eastern Alps, *Tectonophysics*, 280, 267–293, 1997.
- 640 Froitzheim, N., Schmid, S. M., and Conti, P.: Repeated change from crustal shortening to orogen-parallel extension in the Austroalpine units of Graubünden, *Eclogae Geol. Helv.*, 87(2), 559–612, 1994.
- Fügenschuh, B., Seward, D., Mancktelow, N., and Fumasoli, M.: Exhumation in a convergent orogen: the western Tauern window, *Terra Nova* 9, 213–217, 1997.
- Gillam, B. G., Little, T. A., Smith, E., and Toy, V. G.: Extensional shear band development on the outer margin of the Alpine mylonite zone, Tattare Stream, Southern Alps, New Zealand, *J. Struct. Geol.*, 54, 1–20, <https://doi.org/10.1016/j.jsg.2013.06.010>, 2013.
- 645 Godin, L., Grujic, D., Law, R. D., and Searle, M. P.: Channel flow, ductile extrusion and exhumation in continental collision zones: an introduction. In: Channel flow, ductile extrusion and exhumation in continental collision zones (Law, R.D., Searle, M.P. and Godin, L., eds), *Geol. Soc. London Spec. Pub.*, 268, 1–23, 2006.
- Gregnanin, A., and Valle, M.: Deformation and metamorphism in the Austroalpine Ötztal-Stubai complex (part II): Early Alpine evolution in basement and cover, *Boll. Soc. Geol. It.*, 114, 393–409, 1995.
- 650 Guidotti, C. V., and Sassi, F. P.: Miscellaneous isomorphous substitutions in Na-K white micas: a review, with special emphasis to metamorphic micas, *Rend. Lincei. Sci. Fis. Nat.*, 9, 57–78, 1998.
- Habler, G., Thöni, M., and Sölva, H.: Tracing the high pressure stage in the polymetamorphic Texel Complex (Austroalpine basement unit, Eastern Alps): P-T-t-d constraints, *Miner. Petrol.*, 88, 269–296, 2006.
- 655 Habler, G., Thöni, M., and Grasemann, B.: Cretaceous metamorphism in the Austroalpine Matsch Unit (Eastern Alps): the interrelation between deformation and chemical equilibration processes. *Mineral. Petrol.*, 97(3), 149–171, 2009.
- Handy, M., Schmid, S., Bousquet, R., Kissling, E., and Bernoulli, D.: Reconciling plate-tectonic reconstructions of Alpine Tethys with the geological–geophysical record of spreading and subduction in the Alps, *Earth-Sci Rev.*, 102, 121–158, 2010.
- 660 Hanmer, S., Bowring, S., van Breemen, O., and Parrish, R.: Great Slave Lake shear zone, NW Canada: mylonitic record of Early Proterozoic continental convergence, collision and indentation, *J. Struct. Geol.*, 14(7), 757–773, 1992.
- Heim, A.: *Geologie der Schweiz, Band II. Die Schweizer Alpen*. Tauchnitz, Leipzig, 1018 pp., 1922.
- Hoinkes, G., Koller, F., Rantitsch, G., Dachs, E., Höck, V., Neubauer, F., and Schuster, R.: Alpine metamorphism of the Eastern Alps. *Schweiz. Mineral. Petrogr. Mitt.*, 79, 155–181, 1999.
- 665 Hull, J.: Thickness-displacement relationships for deformation zone, *J. Struct. Geol.* 10, 431–435. [https://doi.org/10.1016/0191-8141\(88\)90020-X](https://doi.org/10.1016/0191-8141(88)90020-X), 1988.
- Jamieson, R. A., Beaumont, C., Medvedev, S. and Nguyen, M. H.: Crustal channel flows: 2. Numerical models with implications for metamorphism in the Himalayan-Tibetan orogen, *JGR Solid Earth*, 109(B6), 2004.
- 670 Janak, M., Cornell, D., Froitzheim, N., De Hoog, J. C. M., Broska, I., Vrabec, M., & Hurai, V.: Eclogite hosting metapelites from the Pohorje Mountains (Eastern Alps): P-T evolution, zircon geochronology and tectonic implications, *Eur. J. Mineral.*, 21, 1191–1212, 2009.

- Klug, L., and Froitzheim, N.: Reuniting the Ötztal Nappe: the tectonic evolution of the Schneeberg Complex, *Int. J. Earth Sci.*, 111(2), 525–542, 2022.
- 675 Koltai, G., Cheng, H., & Spötl, C.: Palaeoclimate significance of speleothems in crystalline rocks: a test case from the Late Glacial and early Holocene (Vinschgau, northern Italy), *Climate of the Past*, 14(3), 369–381, 2018.
- Konzett, J., and Hoinkes, G.: Paragonite-hornblende assemblages and their petrological significance: an example from the Austroalpine Schneeberg Complex, Southern Tyrol, Italy, *J. Metamorph. Geol.*, 14, 85–101, 1996.
- Krenn, K., Kurz, W., Fritz, H., and Hoinkes, G.: Eoalpine tectonics of the Eastern Alps: implications from the evolution of monometamorphic Austroalpine units (Schneeberg and Radenthein Complex), *Swiss J. Geosci.*, 104, 471–491, 2011.
- 680 Kurz, G. A., and Northrup, C. J., 2008. Structural analysis of mylonitic rocks in the Cougar Creek Complex, Oregon–Idaho using the porphyroclast hyperbolic distribution method, and potential use of SC'-type extensional shear bands as quantitative vorticity indicators, *J. Struct. Geol.*, 30, 1005–1012. <https://doi.org/10.1016/j.jsg.2008.04.003>.
- 685 Law, R. D., Stahr, D. W., Francis, M. K., Ashley, K. T., Grasemann, B., and Ahmad, T.: Deformation temperatures and flow vorticities near the base of the Greater Himalayan Series, Sutlej valley and Shimla Klippe, NW India, *J. Struct. Geol.*, 54, 21–53, <https://doi.org/10.1016/j.jsg.2013.05.009>, 2013.
- Lünsdorf, N.K., Dunkl, I., Schmidt, B.C., Rantitsch, G., and Eynatten H.: The thermal history of the Steinach Nappe (Eastern Alps) during extension along the Brenner Normal Fault system indicated by organic maturation and zircon (U-Th)/He thermochronology, *Austrian J. Earth. Sci.*, 105, 17–25, 2012.
- 690 Manatschal, G., and Bernoulli, D.: Architecture and tectonic evolution of nonvolcanic margins: present-day Galicia and ancient Adria, *Tectonics*, 18, 1099–1119, 1999.
- Mancktelow, N. S.: The Simplon Line: a major displacement zone in the western Lepontine Alps, *Eclogae Geol. Helv.*, 78, 73–96, 1985.
- Means, W. D.: Shear zones and rock history, *Tectonophysics*, 247, 157–160. [https://doi.org/10.1016/0040-1951\(95\)98214-H](https://doi.org/10.1016/0040-1951(95)98214-H), 1995.
- 695 Miller, C., Mundil, R., Thöni, M., and Konzett, J.: Refining the timing of eclogite facies metamorphism: a geochemical, petrological, Sm–Nd and U–Pb case study from the Pohorje Mountain, Slovenia (Eastern Alps), *Contrib. Miner. Petrol.*, 150:70–84, 2005.
- Mitra, G.: Deformation of granitic basement rocks along fault zones at shallow to intermediate crustal levels. In: S. Mitra and G. W. Fisher (Editors), *Structural Geology of Fold and Thrust Belts*, Johns Hopkins University Press, Baltimore, MD, pp. 123–144, 1992.
- 700 Montemagni, C.: *Geochronology and Kinematics of Crustal Scale Shear Zones in the Himalayan Collisional Belt*, PhD thesis, Università degli Studi di Milano – Bicocca, 2020.
- Montemagni, C., and Zanchetta, S. : Constraining kinematic and temporal evolution of a normal-sense shear zone: Insights into the Simplon Shear Zone (Western Alps), *J. Struct. Geol.*, 156, 104557, 2022.
- 705 Montemagni, C., and Villa, I. M.: Geochronology of Himalayan shear zones: unravelling the timing of thrusting from structurally complex fault rocks. *J. Geol. Soc. London* <https://doi.org/10.1144/jgs2020-235>, 2021.
- Montomoli, C., Iaccarino, S., Carosi, R., Langone, A., and Visonà, D.: Tectonometamorphic discontinuities within the Greater Himalayan Sequence in Western Nepal (Central Himalaya): Insights on the exhumation of crystalline rocks, *Tectonophysics*, 608, 1349–1370, 2013.

- 710 Montomoli, C., Carosi, R., and Iaccarino, S.: Tectonometamorphic discontinuities in the Greater Himalayan Sequence: a local or a regional feature? In: *Tectonics of the Himalaya* (Mukherjee S., van der Beek, P. and Mukherjee, P.K., eds). Geol. Soc. London Spec. Publ., 412, 21-41, 2015.
- Neubauer, F., Genser, J., and Handler, R.: The Eastern Alps: Result of a two stage collision process, *Mitt. Österr., Geol. Ges.*, 92, 117–134, 2000.
- 715 Oriolo, S., Oyhantçabal, P., Wemmer, K., Heidelbach, F., Pfander, J., Basei, M. A. S., Hueck, M., Hannich, F., Sperner, B., and Siegesmund, S.: Shear zone evolution and timing of deformation in the Neoproterozoic transpressional Dom Feliciano Belt, Uruguay, *J. Struct. Geol.*, 92, 59–78. <https://doi.org/10.1016/j.jsg.2016.09.010>, 2016.
- Oriolo, S., Wemmer, K., Oyhantçabal, P., Fossen, H., Schulz, B., and Siegesmund, S.: Geochronology of shear zones – a review, *Earth Sci. Rev.* 185, 665–683. <https://doi.org/10.1016/j.earscirev.2018.07.007>, 2018.
- 720 Passchier, C.W., and Trouw, R.A.J.: *Microtectonics*. Springer Verlag, Berlin, 2005.
- Petroccia, A., Carosi, R., Montomoli, C., Iaccarino, S., and Brovarone, A. V.: Deformation and temperature variation along thrust-sense shear zones in the hinterland-foreland transition zone of collisional settings: A case study from the Barbagia Thrust (Sardinia, Italy), *J. Struct. Geol.*, 104640, 2022.
- Poli, S.: Reaction spaces and P–T paths: from the amphibole eclogite to the greenschist facies in the Austroalpine domain (Oetztal Complex), *Contrib. Miner. Petrol.*, 106, 399–416, 1991.
- 725 Pomella, H., Flöss, D., Speckbacher, R., Tropper, P., and Fügenschuh, B.: The western end of the Eoalpine High-Pressure Belt (Texel unit, South Tyrol/Italy), *Terra Nova* 28:60–69. <https://doi.org/10.1111/ter.12191>, 2016.
- Purtscheller, F., and Rammlmair, D.: Alpine metamorphism of diabase dikes in the € Oetzal-Stubai metamorphic complex, *Tschermaks Mineral. Petrogr. Mitt.*, 29, 205–221, 1982.
- 730 Ratschbacher, L.: Kinematics of Austro-Alpine cover nappes; changing translation path due to transpression, *Tectonophysics*, 125(4), 335–356, 1986.
- Ratschbacher, L., Neubauer, F., Frisch, W., Schmid, S.M., and Neugebauer, J.: Extension in compressional orogenic belts: The eastern Alps, *Geology*, 17, 404–407, 1989.
- 735 Rockenschaub, M., Kolenprat B., and Frank, W.: Geochronologische Daten aus dem Brennergebiet: Steinacher Decke, Brennermesozoikum, Ötz-Stubai-Kristallin, Innsbrucker Quartzphyllitcomplex, Tarentaler Mesozoikum, Arbeitstagung GSA, Blatt 148 Brenner, 2003.
- Rosenberg, C. L., Schneider, S., Scharf, A., Bertrand, A., Hammerschmidt, K., Rabaute, A., and Brun, J.P.: Relating collisional kinematics to exhumation processes in the Eastern Alps, *Earth Sci. Rev.* 176, 311–344. <https://doi.org/10.1016/j.earscirev.2017.10.013>, 2018.
- 740 Schmid, S. M., Zingg, A., and Handy, M.: The kinematics of movements along the Insubric Line and the emplacement of the Ivrea Zone, *Tectonophysics*, 135, 47–66, 1987.
- Schmid, S. M., Aebli, H. R., Heller, F., Zingg, A., Coward, M. P., Dietrich, D., and Park, R. G.: The role of the Periadriatic Line in the tectonic evolution of the Alps Alpine Tectonics, *Geol. Soc. London, Spec. Pub.*, 45, 153–171, 1989.
- 745 Schmid, S. M., and Haas, R.: Transition from near-surface thrusting to intrabasement decollement, Schlinig Thrust, Eastern Alps, *Tectonics*, 8, 697–718. <https://doi.org/10.1029/TC008i004p00697>, 1989.
- Schmid, S. M., Fügenschuh, B., Kissling, E., and Schuster, R.: Tectonic map and overall architecture of the Alpine orogen, *Eclogae Geol. Helv.*, 97, 93–117, 2004.

- Schoene, B., and Bowring, S. A.: U–Pb systematics of the McClure Mountain syenite: thermochronological constraints on the age of the $^{40}\text{Ar}/^{39}\text{Ar}$ standard MMhb, *Contrib. Mineral. Petrol.* 151, 615–630. <https://doi.org/10.1007/s00410-006-0077-4>, 2006.
- Schulz, B. and Krause, J.: Electron probe petrochronology of polymetamorphic garnet micaschists in the lower nappe units of the Austroalpine Saualpe basement (Carinthia, Austria), *Z. Dt. Ges. Geowiss.* DOI: 10.1127/zdgg/2021/0247, 2021.
- Searle, M. P., Law, R. D., Godin, L., Larson, K. P., Streule, M. J., Cottle, J. M. & Jessup, M. J., 2008. Defining the Himalayan Main Central Thrust in Nepal. *Journal of the Geological Society, London*, 165, 523-534.
- Simpson, C., and De Paor, D. G.: Strain and kinematic analysis in general shear zones, *J. Struct. Geol.*, 15(1), 1–20, 1993.
- Sölva, H., Grasemann, B., Thöni, M., Thiede, R., Habler, G.: The Schneeberg normal fault zone: normal faulting associated with Cretaceous SE-directed extrusion in the Eastern Alps (Italy/Austria), *Tectonophysics*, 410, 143–166, 2005.
- Spitz, A., and Dyrenfurth, G.: Monographie der Engadiner Dolomiten zwischen Schuls, Scansf und der Stilfserjoch. *Beitr. geol. Karte Schweiz (NF) 44*, 1914.
- Staub, R.: Geologische Probleme zwischen Engadin und Ortler, *Denkschr. Schweiz. Naturf. Ges.*, 72, 1-115, 1937.
- Steiger, R., and Jäger, E.: Subcommittee on geochronology: convention on the use of decay constants in geo- and cosmochronology, *Earth Planet. Sci. Lett.*, 36, 359-362, 1977.
- Stipp, M., Stunitz, H., Heilbronner, R. and Schmid, S. M.: The eastern Tonale fault zone: A natural laboratory for crystal plastic deformation over a temperature range from 250 to 700 °C, *J. Struct. Geol.*, 24, 1861–1884, 2002.
- Stübner, K., Ratschbacher, L., Weise, C., Chow, J., Hofmann, J., Khan, J., ... & Project TIPAGE members: The giant Shakh-dara migmatitic gneiss dome, Pamir, India-Asia collision zone: 2. Timing of dome formation, *Tectonics*, 32(5), 1404-1431, 2013.
- Thöni, M.: Distribution of pre-Alpine and Alpine metamorphism of the southern Ötztal Mass and the Scarl Unit, based on K/Ar age determinations, *Mitt. österr. geol. Ges.*, 71(72), 139-165, 1980.
- Thöni, M.: The Rb-Sr thin slab isochron Method-an Unreliable Geochronologic Method for Dating Geologic Events in Polymetamorphic Terrains?: Evidence from the Austroalpine Basement Nappe, the Eastern Alps, *Mem. Soc. Geol.*, 38, 283–352, 1986.
- Thöni, M.: A review of geochronological data from the Eastern Alps. *Schweiz. Mineral. Petrogr. Mitt.*, 79, 209–230, 1999.
- Thöni, M.: Sm–Nd isotope systematics in garnet from different lithologies (Eastern Alps): age results, and an evaluation of potential problems for garnet Sm–Nd chronometry, *Chem. Geol.*, 185, 255–281. [https://doi.org/10.1016/S0009-2541\(02\)00419-9](https://doi.org/10.1016/S0009-2541(02)00419-9), 2002.
- Thöni, M., Miller, C., Blichert-Toft, J., Whitehouse, M. J., Konzett, J., and Zanetti, A.: Timing of high-pressure metamorphism and exhumation of the eclogite-type locality (Klupperbrunn-Prickler Halt, south-eastern Austria): constraints from the correlation of the Sm–Nd, Lu–Hf, U–Pb and Rb–Sr isotopic systems, *J. Metamorph. Geol.*, 26, 561–581, 2008.
- Tropper, P. and Reicheis, A.: Garnet zoning as a window into the metamorphic evolution of a crystalline complex: the northern and central Austroalpine Ötztal-Complex as a polymetamorphic example, *Mitt. Osterr. Geol. Ges.*, 94, 27–53, 2003.
- Villa, I.M.: The in vacuo release of Ar from minerals: 1. Hydrous minerals. *Chem. Geol.*, 564, 120076, 2021.

- Viola, G., Mancktelow, N.S., Seward, D., Meier, A., and Martin, S.: The Pejo fault system: an example of multiple tectonic activity in the Italian Eastern Alps, *GSA Bull.*, 115, 515–532, 2003.
- 790 Vitale, S., and Mazzoli, S.: Heterogeneous shear zone evolution: the role of shear strain hardening/softening, *J. Struct. Geol.*, 30, 1383–1395. <https://doi.org/10.1016/j.jsg.2008.07.006>, 2008.
- Vitale, S., and Mazzoli, S.: Strain analysis of heterogeneous ductile shear zones based on the attitudes of planar markers, *J. Struct. Geol.*, 32(3), 321–329, 2010.
- Xypolias, P., and Koukouvelas, I. K.: Kinematic vorticity and strain rate patterns associated with ductile extrusion in the Chelmos Shear Zone (External Hellenides, Greece), *Tectonophysics*, 338(1), 59–77, 2001.
- 795 Xypolias, P.: Vorticity analysis in shear zones: a review of methods and applications, *J. Struct. Geol.*, 32, 2072–2092. <https://doi.org/10.1016/j.jsg.2010.08.009>, 2010.
- Wiesinger, M., Neubauer, F., Handler, R.: Exhumation of the Saualpe eclogite unit, Eastern Alps: constraints from $^{40}\text{Ar}/^{39}\text{Ar}$ ages, *Mineral. Petrol.*, 88, 149–180, 2006.
- 800 Zanchetta, S., D’Adda, P., Zanchi, A., Barberini, V., and Villa, I.M.: Cretaceous-Eocene compression in the central Southern Alps (N Italy) inferred from $^{40}\text{Ar}/^{39}\text{Ar}$ dating of pseudotachylytes along regional thrust faults, *J. Geodyn.*, 51(4), 245–263, 2011.
- Zanchetta, S., Garzanti, E., Doglioni, C. and Zanchi, A.: The Alps in the Cretaceous: a doubly vergent pre-collisional orogen, *Terra Nova*, 24(5), 351–356, 2012.
- 805 Zanchetta, S., Poli, S., Rubatto, D., Zanchi, A., and Bove, G.: Evidence for deep subduction of Austroalpine crust (Texel Complex, NE Italy), *Rend. Fis. Acc. Lincei.*, 24, 163–176. <https://doi.org/10.1007/s12210-013-0239-z>, 2013.
- Zanchetta, S., Malusà, M. G., and Zanchi, A.: Precollisional development and Cenozoic evolution of the Southalpine retrobelt (European Alps), *Lithosphere*, 7(6), 662–681, 2015.
- Zantedeschi, C.: Geocronologia Rb–Sr sugli gneiss granitoidi del Complesso di Parcines (Alto Adige Occidentale), *Mem. Sci. Geol.*, 43, 319–329, 1991.
- 810

Supplementary Table 1: sample list with coordinates in UTM32N and elevation m a.s.l.

815 **Supplementary Table 2: Electron probe micro analyses of micas (wt% oxides). Atomic proportions (apfu) were recalculated based on 11 oxygens.**

Supplementary Table 3: $^{40}\text{Ar}/^{39}\text{Ar}$ data. All Ar isotope concentrations are given as mL. K, Ca and Cl concentrations are calculated from the sample mass and the ^{39}Ar , ^{37}Ar and ^{38}Ar concentrations, respectively.